

Deep Reinforcement Learning Approach to QoS-Aware Load Balancing in 5G Cellular Networks under User Mobility and Observation Uncertainty

M. Eskandarpour, H. Soleimani

School of Electrical Engineering, Iran University of Science & Technology (IUST), Tehran, Iran

Corresponding Author: hsoleimani@iust.ac.ir

Abstract— Efficient mobility management and load balancing are critical to sustaining Quality of Service (QoS) in dense, highly dynamic 5G radio access networks. We present a deep reinforcement learning framework based on Proximal Policy Optimization (PPO) for autonomous, QoS-aware load balancing implemented end-to-end in a lightweight, pure-Python simulation environment. The control problem is formulated as a Markov Decision Process in which the agent periodically adjusts Cell Individual Offset (CIO) values to steer user-cell associations. A multi-objective reward captures key performance indicators—aggregate throughput, latency, jitter, packet loss rate, Jain’s fairness index, and handover count—so the learned policy explicitly balances efficiency and stability under user mobility and noisy observations. The PPO agent uses an actor-critic neural network trained from trajectories generated by the Python simulator with configurable mobility (Gauss–Markov) and stochastic measurement noise. Across 500+ training episodes and stress tests with increasing user density, the PPO policy consistently improves KPI trends (higher throughput and fairness, lower delay, jitter, packet loss, and handovers) and exhibits rapid, stable convergence. Comparative evaluations show that PPO outperforms rule-based ReBuHa and A3 as well as the learning-based CDQL baseline across all KPIs while maintaining smoother learning dynamics and stronger generalization as load increases. These results indicate that PPO’s clipped policy updates and advantage-based training yield robust, deployable control for next-generation RAN load balancing using an entirely Python-based toolchain.

Index Terms— 5G Networks, Load Balancing, Deep Reinforcement Learning, PPO, Mobility Management.

I. INTRODUCTION

The rapid expansion of mobile services [1] and the growing demand [2] for bandwidth-intensive [3], latency-sensitive applications [4] have transformed the landscape of wireless communications [5]. Technologies such as ultra-high-definition video streaming, augmented/virtual reality (AR/VR), autonomous driving [6], and massive Internet of Things (IoT) deployments place unprecedented stress on cellular infrastructure [7]. To meet these expectations, fifth-generation

(5G) networks must deliver higher capacity and lower latency while providing reliable [8], intelligent resource allocation [9] across dense and dynamic Radio Access Networks (RANs) [10]. Within this context, effective load balancing is central to sustaining Quality of Service (QoS) [11], maximizing spectral efficiency, and preserving user experience under heterogeneous traffic and mobility patterns [12].

Conventional mobility control—exemplified by A3-based handover [13]—compares downlink signal strength indicators (e.g., RSRP) against fixed thresholds [14] such as hysteresis and Time-To-Trigger (TTT) [15]. While simple and deployable, these policies struggle to adapt to rapid topology and traffic changes and generally ignore end-to-end QoS indicators [16] (delay, jitter, packet loss) and system-level fairness [17]. Resource-aware heuristics such as ReBuHa incorporate load proxies like Resource Block Utilization (RBU) [18], but remain rule-based and brittle under high user mobility, stochastic traffic, and noisy/partial observations [19].

These limitations have motivated the application of Reinforcement Learning (RL) [20] to network self-optimization, where agents learn sequential decision policies from interaction feedback [21]. Among policy-gradient methods, Proximal Policy Optimization (PPO) has emerged as a practical, stable on-policy algorithm with strong empirical performance across continuous and discrete control tasks [22], [23]. PPO’s clipped surrogate objective constrains policy updates, its advantage-based training reduces variance, and entropy regularization encourages exploration—all desirable properties for non-stationary, noisy wireless environments with competing objectives.

In this paper, we adopt PPO to optimize QoS-aware load balancing in dense 5G-like RANs using a pure-Python simulation environment. The control problem is formulated as a Markov Decision Process (MDP) in which the agent periodically adjusts Cell Individual Offset (CIO) parameters to steer user-cell associations. The state aggregates per-cell and per-user measurements (load, RSRP/CQI summaries, queueing/latency statistics, recent handovers). The action is a

vector of CIO adjustments subject to operational bounds. The reward is a multi-objective signal that simultaneously captures six KPIs—aggregate throughput, latency, jitter, packet loss rate, Jain’s fairness index, and handover count—thereby aligning short-term decisions with long-term service quality and stability. User mobility follows configurable stochastic models (e.g., Gauss–Markov), and measurements are corrupted with controlled noise to emulate realistic observability.

We further benchmark PPO against two classical baselines (A3 and ReBuHa) and a learning-based baseline (CDQL), using identical traffic, mobility, and noise settings for fairness. Across 500+ training episodes and stress tests with increasing user density, PPO consistently yields higher throughput and fairness and lower delay, jitter, packet loss, and handover frequency, exhibiting smooth and robust convergence in the presence of measurement noise. While CDQL improves upon rule-based schemes, PPO remains superior across all KPIs in our setting, highlighting the advantages of clipped policy updates and advantage learning for this task. Contributions:

- (1) PPO-driven load balancing for 5G RANs: We design an actor–critic controller that adaptively tunes CIO values to orchestrate user association under mobility.
- (2) Multi-objective QoS reward: We craft a composite reward over six KPIs (throughput, latency, jitter, packet loss, fairness, handovers) to explicitly trade off efficiency and stability.
- (3) Realism via mobility and noise: We evaluate under Gauss–Markov mobility and stochastic measurement noise, demonstrating robustness to partial observability.
- (4) Pure-Python toolchain: The entire framework—environment, training loop, and evaluation—is implemented in Python, facilitating reproducibility and rapid experimentation.
- (5) Comprehensive benchmarking: We compare PPO with A3, ReBuHa, and CDQL; PPO achieves the best overall QoS and convergence behavior across all experiments.

Organization. The remainder of the paper is structured as follows. Section II reviews related work in RAN load balancing and RL for network control. Section III presents the system model and MDP formulation. Section IV details the PPO methodology, including network architecture, advantage estimation, and training pipeline. Section V describes the simulation setup and reports results across KPIs and user densities. Section VI concludes and outlines future directions.

II. RELATED WORK

We review two closely related strands: (i) load balancing via handover (HO)/cell-selection mechanisms in RANs—our main focus—and (ii) power-control methods that often co-optimize with load and mobility in 5G V2X systems. We emphasize RL-based approaches and mmWave small-cell deployments relevant to vehicular users. Because load balancing strongly

affects resource savings and end-to-end performance, many studies tackle it by adapting HO strategies—either tuning HO parameters or continuously tracking KPIs (e.g., [24], [25]). More recently, ML has been applied to mobility/load decisions: (i) a Q-learning 5G HO that selects data-link and access beams to optimize mobility [26]; (ii) supervised deep learning that uses SINR variation to predict radio-link failure (RLF) probability and hand over to the cell with lower predicted RLF [27]; (iii) an RL-based mobility load balancing (MLB) framework for ultra-dense networks with a two-layer design—cluster formation followed by per-cluster MLB that sets HO parameters by minimizing PRB utilization [28]; and (iv) an RL-based LTE load-balancing scheme that maximizes instantaneous network throughput [29]. Unlike these works, we explicitly incorporate QoS metrics—including delay and channel quality—alongside resource-block utilization, seeking to balance both while maximizing overall performance.

Power allocation has been explored for autonomous-vehicle scenarios across multiple link types, including UAV–vehicle and inter-vehicle links. UAV-assisted vehicular downlink power allocation to maximize per-UAV throughput has been investigated [30]. For V2V, PPO has been used for joint power and bandwidth allocation, modeling each link (vehicle) as an agent [31]. A centralized hierarchical DRL at the RSU has been proposed for relay selection and power allocation across sub-6 GHz (coverage) and mmWave (high-rate) bands in multi-hop vehicular networks [32]. For D2D transmission, a GNN-based power-control method targets weighted sum-rate maximization [33].

Downlink cellular power allocation. Although our focus is downlink load balancing/association, a substantial body of work optimizes downlink power: joint power/channel assignment in multi-AP WLANs via Q-learning [34]; joint HO control and power allocation using multi-agent PPO with centralized training in macro + mmWave small-cell layouts to improve throughput and reduce handovers [35]; mmWave small-cell resource management for sum-rate maximization via sub-optimal heuristics [36]; user association plus power control in ultra-dense mmWave small cells with Q-learning [37]; and spectrum–power allocation that trades off spectral/energy efficiency and fairness using DRL in ultra-dense networks [38]. Power control coupled with caching for vehicular video delivery in macro + mmWave small cells has been optimized with DDPG in downlink settings [39].

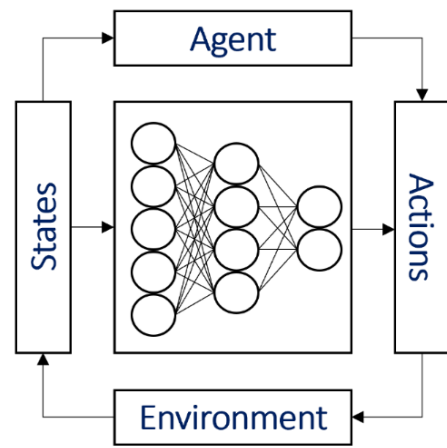
Uplink power control for cellular users (vehicles → gNB) is commonly centralized or distributed [40]. Centralized schemes aggregate network state at the gNB, jointly optimize all users’ transmit powers, and signal decisions—enabling explicit interference management at the cost of higher control-plane overhead. Distributed schemes rely on per-user decisions with local observations; some leverage federated learning to periodically aggregate user-trained models at the BS.

Representative studies include multi-agent DDPG for uplink power allocation/beamforming in mmWave high-speed rail systems [41]; stateless Q-learning for SDN-assisted MEC architectures that jointly optimize uplink power, sub-channel assignment, and offloading [42]; federated DQN across macro + small cells balancing throughput and power consumption under QoS constraints [43]; and uplink resource allocation for high-reliability, low-latency vehicular communications with packet retransmissions [44]. Power control and beamforming for both uplink and downlink have been extensively studied [45]–[49]. An optimization-based design that jointly selects transmit power and the beamforming vector to maximize SINR is presented in [49], though it ignores scattering and shadowing effects that are central to mmWave propagation. LTE introduced almost blank subframes (ABS) to mitigate co-channel inter-cell interference when neighboring base stations (BSs) collide [50]. However, ABS is less effective with dynamic beamforming, which continually changes spatial patterns [51]. Online learning for MIMO link adaptation has been explored with computational complexity comparable to other online approaches and low spatial overhead [52]. Interference avoidance in heterogeneous networks has also been tackled via Q-learning, enabling decentralized self-organization of macro–femto coexistence and reducing femto-to-macro interference [53]. A related Q-learning framework for packetized-voice power control in indoor multi-cell settings leverages semi-persistent scheduling to emulate a dedicated channel and outperform fixed-power schemes on voice quality [54]. Joint power control for massive MIMO can reduce overhead by limiting CSI exchange among cooperating BSs, improving SINR [46]. For uplink power control with beamforming, optimization formulations maximize the achievable sum-rate under per-user minimum-rate constraints [47]. While reinforcement learning could be applied to such uplink problems, it may be computationally costly and energy-hungry for user equipment (UEs); many works therefore emphasize downlink control and/or interference cancellation alongside power control and beamforming. Recent deep learning efforts in wireless span multiple tasks [55]–[61]. In mmWave systems, deep reinforcement learning has been used for power control as an alternative to beamforming to improve NLOS performance, casting power allocation as a Q-learning problem with a convolutional approximation of the action-value function [48]. Deep Q-learning has also been used to maximize successful transmissions in dynamic, correlated multi-channel access environments [55], and deep convolutional networks have improved automatic modulation recognition at low SINR in cognitive radio scenarios [56]. For beam management, deep neural networks can predict mmWave beams from omnidirectional signals gathered at neighboring BSs [60], and can even map limited channel knowledge at a small array to an SINR-optimal beamformer for a larger array—potentially at a

different frequency and at a neighboring BS [61]. Deep learning has also been used to synthesize antenna patterns achieving near-optimal SINR for data bearers [62], though without explicit power control or inter-cell coordination. RL-based automated cellular network tuning has been demonstrated in heterogeneous settings [63]. Joint beam management and interference coordination at mmWave with deep networks often assumes channel knowledge at inference [64]. Finally, deep learning-based downlink beamforming optimization without reinforcement learning has been studied in MISO systems [65]. Our study is closest to [66]. Both works pursue QoS-aware load balancing with a multi-KPI reward that explicitly accounts for user experience under mobility. However, they adopt a value-based CDQL controller and a general wireless-network setting, whereas we develop a policy-gradient PPO controller tailored to 5G RAN with mmWave small cells and vehicular mobility. Concretely, our method (i) operates through bounded CIO adjustments for user–cell association, (ii) optimizes a broader QoS set (throughput, delay, jitter, loss, fairness, and handovers) with action-smoothness regularization, and (iii) analyzes robustness under observation lag, noise, and missingness—aspects not covered by the CDQL study. These differences make our approach better aligned with near-RT RIC implementation constraints in modern 5G deployments.

III. SYSTEM MODEL

In this section, we present the architecture of the cellular network under study, describe the user mobility and observation models, and formulate the load balancing problem as a Markov Decision Process (MDP) suitable for deep reinforcement learning. Our goal is to design an intelligent agent that dynamically adjusts handover bias values to optimize overall network performance in terms of multiple QoS metrics, under realistic assumptions of user mobility and noisy observations.



$\Psi = \{UE_1, UE_2, UE_3, \dots, UE_N\}$ user equipments moving in a two-dimensional area. Each BS operates over bandwidth B MHz, partitioned into R resource blocks. At each decision step t , every UE is associated to one BS and reports radio and QoS statistics (e.g., RSRP/RSRQ/CQI, delay, loss) to its serving BS. A QoS-aware MAC scheduler assigns RBs prioritizing head-of-line (HOL) delay and instantaneous channel quality.

We denote the control interval by ΔT . Within each ΔT , the controller computes CIO biases that influence RRC handover logic in the underlying network.

Mobility Model (Gauss–Markov)

To generate realistic user motion with temporal correlation, we adopt the Gauss–Markov mobility model, in which each UE’s speed v_t and heading angle θ_t evolve as first-order autoregressive processes. The key idea is that the UE does not restart its motion randomly at each step; instead, the current speed and direction are partly inherited from the previous step and partly pulled toward long-term mean values \bar{v} and $\bar{\theta}$, with an additional random perturbation. This produces smooth trajectories with inertia-like behavior, which is closer to pedestrian or vehicular motion than memoryless random walks. Formally, the model updates speed and heading according to

$$v_t = \alpha v_{t-1} + (1 - \alpha)\bar{v} + \sqrt{1 - \alpha^2} \delta_v \quad (1)$$

$$\theta_t = \alpha \theta_{t-1} + (1 - \alpha)\bar{\theta} + \sqrt{1 - \alpha^2} \delta_\theta \quad (2)$$

where $\delta_v \sim \mathcal{N}(0, \sigma_v^2)$ and $\delta_\theta \sim \mathcal{N}(0, \sigma_\theta^2)$, and $\alpha \in [0, 1]$ controls the temporal memory. When α is small, the process becomes weakly correlated and the UE may change its speed or direction abruptly; as α approaches one, the updates become strongly correlated over time, leading to gradual accelerations and smooth turns. The terms $(1 - \alpha)\bar{v}$ and $(1 - \alpha)\bar{\theta}$ ensure mean reversion toward typical speed and preferred direction, while the factor $\sqrt{1 - \alpha^2}$ scales the innovation noise so that the variability of the process remains well-behaved as α changes, rather than shrinking unrealistically when the memory increases.

Given v_t and θ_t , the UE’s position is updated in continuous 2D space using standard kinematics with a simulation step Δt :

$$x_t = x_{t-1} + v_t \Delta t \cos(\theta_t) \quad (3)$$

$$y_t = y_{t-1} + v_t \Delta t \sin(\theta_t) \quad (4)$$

In practice, speed is constrained to physically meaningful values (e.g., nonnegative and bounded by a maximum), and θ_t is wrapped to a valid angular range (e.g., $(-\pi, \pi]$ or $[0, 2\pi)$) to

avoid discontinuities in trigonometric updates. These common constraints prevent unrealistic spikes and keep trajectories stable over long simulation horizons.

This mobility choice is particularly important for studying load balancing under mobility because it induces nontrivial, time-correlated handover behavior. As UEs move smoothly across the coverage regions of neighboring gNBs, their received signal strength and SINR typically change gradually, which yields more realistic transitions in association decisions than abrupt, uncorrelated jumps. Moreover, the correlated motion can cause UEs to graze cell borders or traverse along boundary regions, which increases the likelihood of repeated border crossings and potential ping-pong tendencies in association if hysteresis or TTT effects are considered. These patterns, combined with heterogeneous UE speeds and turning variability, generate dynamic and uneven traffic distributions over cells and time, making the QoS-aware load balancing problem more representative of real deployments.

Observation Model with Noise

In practical 5G RAN control, the decision-maker never has access to a perfectly accurate and perfectly up-to-date network state. The quantities used as inputs to a load-balancing controller—such as RSRP, CQI, and delay-related statistics—are all obtained through a measurement and reporting pipeline that introduces uncertainty. RSRP is estimated from reference signals and is influenced by receiver noise, interference fluctuations, fast fading, and implementation-specific measurement windows. CQI is derived from SINR-related measurements and is typically reported with limited resolution and at finite periodicity, often after link adaptation and scheduler interactions that already average or mask rapid variations. Delay metrics are even more indirect: they are computed from queueing and packet timing counters that are aggregated over time windows, can be quantized in telemetry systems, and may reach the controller with reporting latency. Training an RL agent on idealized observations can therefore lead to policies that rely on unrealistically fine-grained state information and degrade sharply when deployed under measurement error and stale reporting. To avoid this mismatch and to explicitly study robustness, we model the agent’s observation as a corrupted version of the true per-BS aggregates, thereby capturing a partially observed control setting that is closer to operational conditions.

Let x_t denote a generic per-base-station aggregate at decision epoch t (e.g., average RSRP across UEs currently served by that BS, mean CQI, or average packet delay). Rather than feeding x_t directly to the learning agent, we construct an observed channel \tilde{x}_t that accounts for imperfections in estimation, quantization, and asynchronous reporting. In our model, this uncertainty is

represented through additive Gaussian perturbations applied to key inputs:

$$\widetilde{\text{RSRP}}_t = \text{RSRP}_t + \epsilon_t^{\text{RSRP}}, \epsilon_t^{\text{RSRP}} \sim \mathcal{N}(0, \sigma_{\text{RSRP}}^2) \quad (5)$$

$$\widetilde{\text{CQI}}_t = \text{CQI}_t + \epsilon_t^{\text{CQI}}, \epsilon_t^{\text{CQI}} \sim \mathcal{N}(0, \sigma_{\text{CQI}}^2) \quad (6)$$

$$\widetilde{D}_{\text{avg},t} = D_{\text{avg},t} + \epsilon_t^D, \epsilon_t^D \sim \mathcal{N}(0, \sigma_D^2) \quad (7)$$

This additive form is a compact surrogate for multiple real-world error sources that collectively behave like approximately zero-mean disturbances. In particular, when the reported metric is itself an aggregate over UEs and/or over a reporting window, the resulting error often becomes approximately Gaussian due to the accumulation of many small independent components (a standard central-limit effect). It also provides a controllable, interpretable way to stress-test the policy by varying $\sigma_{\text{RSRP}}, \sigma_{\text{CQI}}, \sigma_D$, thereby sweeping from lightly corrupted telemetry to more challenging observation uncertainty.

Because the underlying quantities have physical domains and standard reporting conventions, the corrupted observations are post-processed to remain realistic. RSRP is typically expressed in dB-like units, where small additive perturbations correspond naturally to measurement error. CQI, however, is commonly an integer-valued index within a bounded range (depending on the system configuration). After adding noise, we therefore map CQI back to a valid domain by applying rounding and clipping, ensuring the observation remains consistent with a quantized feedback channel. Likewise, delay-related metrics are constrained to be nonnegative, since negative queueing delay has no physical meaning; any noise-induced negative values are truncated to zero. These validity constraints are important in journal-grade simulation methodology because they prevent the learning agent from seeing impossible inputs and they keep the observation distribution aligned with what a real controller would receive.

Beyond instantaneous corruption, a major practical issue is that network telemetry is rarely synchronized with the control loop. Base-station aggregates are typically computed over finite windows and reported periodically, meaning that the controller effectively observes a smoothed and slightly stale version of the true state. To emulate this effect, we apply light temporal filtering to each noisy observation channel before presenting it to the policy network. Using an exponential moving average, the filtered observation \hat{x}_t is computed as

$$\hat{x}_t = \lambda \hat{x}_{t-1} + (1 - \lambda) \tilde{x}_t, \quad 0 \leq \lambda < 1 \quad (8)$$

where λ controls the strength of smoothing. When λ is close to zero, the agent sees nearly instantaneous (though still noisy) measurements. As λ increases, the agent increasingly observes an averaged signal that changes more slowly, which captures the combined effect of measurement windows, reporting periodicity, and mild delays. This filtering also reduces sensitivity to fast fading spikes and short-lived scheduling artifacts, encouraging the agent to base its decisions on persistent trends rather than transient fluctuations. In the context of QoS-aware load balancing, this is particularly relevant because association decisions and load redistribution typically operate on slower time scales than per-TTI channel variations.

Finally, since the observation vector mixes heterogeneous quantities with very different numerical ranges and units, we apply running normalization before feeding the channels to the learning agent. Without normalization, large-magnitude features (for example, raw delay values measured in milliseconds) can dominate neural-network activations and gradients, while bounded indices (such as CQI) may become underutilized. We therefore standardize each filtered channel using online estimates of mean and variance, producing normalized features with approximately comparable scale:

$$z_t = \frac{\hat{x}_t - \mu_t}{\sqrt{s_t^2 + \epsilon}} \quad (9)$$

where μ_t and s_t^2 are running estimates computed from the training stream and ϵ is a small constant for numerical stability. This transformation does not remove uncertainty; it ensures that uncertainty is presented consistently across features and across training time, improving optimization stability and helping the learned policy generalize across different traffic intensities and mobility regimes. For evaluation, the same normalization procedure is applied using the statistics accumulated during training (or frozen statistics), mirroring the standard practice of deploying a trained policy with fixed preprocessing parameters. Overall, this observation model explicitly couples three realism factors that materially affect learning in mobile 5G environments: imperfect measurement (captured via controlled noise injection), stale/averaged telemetry (captured via EMA filtering), and heterogeneous feature scales (handled via running normalization). By training under these conditions, the agent is forced to learn policies that remain effective when the state is only partially observed and when network indicators are noisy and delayed, which is precisely the operating regime of practical RAN load balancing.

MDP Formulation

We cast QoS-aware load balancing and mobility management in the downlink 5G RAN as an episodic MDP $(\mathcal{S}, \mathcal{A}, \mathcal{P}, \mathcal{R}, \gamma)$ operating at a near-real-time control interval

ΔT . At each decision epoch t , the controller receives a network summary computed from UE reports and base-station scheduling outcomes, then selects a control action that modifies cell-selection biases and thereby influences subsequent handover and association behavior. The environment then evolves over the next interval as users move, radio conditions fluctuate, and traffic is served by the QoS-aware scheduler; these dynamics jointly determine the next observed state and the instantaneous reward. This formulation matches the closed-loop nature of the problem: the controller does not directly assign users to cells, but rather steers the association process indirectly via CIO parameters that bias standard RRC handover logic, allowing the policy to continuously redistribute load while respecting mobility and radio constraints.

The underlying network dynamics are Markovian when expressed in terms of the full physical state that includes UE locations and velocities, propagation and fading realizations, traffic arrivals and queue states, and the current handover configuration. In practice, the learning agent observes only aggregated and possibly noisy performance indicators produced over a recent measurement window, which introduces a controlled degree of partial observability. We therefore define the agent's state s_t as the filtered/normalized vector of per-base-station aggregates available at time t , and we treat the induced process over these aggregates as the effective MDP state used for policy learning. This choice is consistent with operational 5G control: UEs periodically report radio and QoS measurements (e.g., RSRP/CQI and delay/loss), base stations summarize these measurements and scheduling outcomes, and the controller acts on the resulting statistics rather than on instantaneous per-packet or per-UE micro-states.

The action space \mathcal{A} consists of a continuous, bounded CIO adjustment vector applied across the M cells, $a_t = [\text{CIO}_1(t), \dots, \text{CIO}_M(t)]$, with each component constrained within predefined limits (e.g., $[\text{CIO}_{\min}, \text{CIO}_{\max}]$). By shifting CIO values, the controller changes the relative attractiveness of cells in overlap regions and alters handover triggering in a load-aware manner, enabling proactive offloading before severe queue build-up occurs while discouraging unnecessary ping-pong events through smooth and selective bias updates.

The transition kernel $\mathcal{P}(s_{t+1} | s_t, a_t)$ is induced by the simulator's coupled mechanisms: user mobility (Gauss-Markov evolution of speed and heading), channel propagation (path loss, shadowing, and small-scale fading), stochastic traffic generation, and resource scheduling decisions that convert available PRBs into served rates and experienced delays. Because CIO actions influence association and handover decisions, they affect PRB utilization, queueing, retransmissions, and ultimately QoS metrics observed in the next control interval. In addition, observation uncertainty is explicitly modeled by injecting noise into key reported inputs and applying light temporal filtering prior to constructing the

agent's state, which makes the learned policy robust to estimation/quantization errors and reporting imperfections. The reward function \mathcal{R} provides a scalar performance signal that encodes multi-objective QoS goals, combining throughput and fairness incentives with penalties on latency, jitter, packet loss, and excessive handovers. Concretely, the instantaneous reward R_t is computed from normalized KPI components (mapped to $[0,1]$ with consistent directionality) and then weighted to reflect target service priorities, so that improvements in user experience and load balance are reinforced while instability and churn are discouraged. This scalarization allows the agent to learn policies that manage inherent trade-offs—such as offloading to relieve congestion at the cost of slightly weaker radio conditions—by optimizing long-term cumulative benefit rather than reacting myopically to instantaneous signal strength.

Finally, the control objective is to learn a policy π^* that maximizes the expected discounted return over each episode, $\mathbb{E}[\sum_{t=0}^{\infty} \gamma^t R(s_t, a_t)]$, with γ chosen close to one to emphasize sustained QoS rather than short-lived gains. In our setup, episodes run for a fixed horizon, which encourages the policy to account for delayed effects of CIO changes on future load distribution, queueing, and mobility outcomes under realistic user motion and noisy measurements.

State

At decision time t the controller observes per-BS aggregates:

$$\eta(t) = [\eta_1(t), \dots, \eta_M(t)] \quad (10)$$

$$T(t) = [\bar{T}_1(t), \dots, \bar{T}_M(t)] \quad (11)$$

$$J(t) = [\bar{J}_1(t), \dots, \bar{J}_M(t)] \quad (12)$$

$$L(t) = [\bar{Latency}_1(t), \dots, \bar{Latency}_M(t)] \quad (13)$$

$$P(t) = [\bar{PLR}_1(t), \dots, \bar{PLR}_M(t)] \quad (14)$$

$$H(t) = [\bar{H}_1(t), \dots, \bar{H}_M(t)] \quad (15)$$

At decision time t , the agent observes for each base station $i = 1, \dots, M$: $\eta_i(t)$, cell utilization, i.e., the fraction of PRBs (or airtime) scheduled over the last window (Eq. 10). $\bar{T}_i(t)$ mean downlink throughput served by BS i over the window (Eq. 11). $\bar{J}_i(t)$ mean jitter, computed as the average absolute inter-packet delay variation for flows served by BS i (Eq. 12). $\bar{Latency}_i(t)$ mean one-way packet delay for BS i (Eq. 13). $\bar{PLR}_i(t)$, packet-loss ratio, fraction of packets dropped for traffic served by BS i (Eq. 14). Optionally, $\bar{H}_i(t)$ summarizes recent handover activity attributable to BS i (Eq. 15). These channels are lightly

filtered and normalized before being stacked as the state s_t . We concatenate these to form:

$$s_t = [\eta(t), T(t), J(t), P(t), L(t), H(t)] \in \mathbb{R}^{6M} \quad (16)$$

All channels may be noisy as above.

Action

The controller sets CIO biases for all BSs:

$$a_t = [CIO_1(t), CIO_2(t), \dots, CIO_M(t)] \quad (17)$$

Each CIO is bounded: $CIO_i(t) \in [CIO_{min}, CIO_{max}]$. CIOs bias attachment decisions and indirectly adjust cell loads.

Reward

We scalarize six QoS goals with tunable weights w_k (normalized unless stated):

$$R_t = w_1 R_{THR}(t) - w_2 R_{JIT}(t) - w_3 R_{LAT}(t) + w_4 R_{JF}(t) - w_5 R_{PLR}(t) - w_6 R_{HO}(t) \quad (18)$$

The components are defined and normalized to [0,1].

$$R_{THR} = \frac{1}{M} \sum_{i=1}^M \bar{T}_i(t) \quad (19)$$

$$R_{JIT} = \frac{1}{M} \sum_{i=1}^M \bar{J}_i(t) \quad (20)$$

$$R_{PLR} = \frac{1}{M} \sum_{i=1}^M \bar{PLR}_i(t) \quad (21)$$

$$R_{LAT} = \frac{1}{M} \sum_{i=1}^M \bar{L}_i(t) \quad (22)$$

$$R_{JF} = \frac{(\sum_i \eta_i(t))^2}{M \cdot \sum_i \eta_i^2(t)} \quad (23)$$

$$R_{HO}(t) = \frac{H(t)}{H_{max}} \quad (24)$$

Throughput term R_{THR} rewards high aggregate cell throughput normalized to a reference maximum; jitter term R_{JIT} penalizes average packet-delay variation across cells (lower is better); packet-loss term R_{PLR} penalizes mean packet-loss ratio across cells (lower is better); latency term R_{LAT} penalizes mean one-way delay across cells (lower is better); fairness term R_{JF} encourages balanced utilization using Jain's index over per-cell load; handover term $R_{HO}(t)$ penalizes total handovers to

discourage ping-pong. These terms are combined in Eq. (15) with weights that sum to 1; KPI directions are normalized where appropriate, and a small action-smoothness penalty is applied elsewhere. Weights $w_k (k = 1, \dots, 6)$ define the relative importance of each KPI, normalized to $\sum w_k = 1$.

Transitions and discount

The transition kernel $P(s_{t+1} | s_t, a_t)$ is induced by the closed-loop network simulator that evolves user locations, radio conditions, traffic/queues, and scheduling outcomes over a discrete decision interval ΔT . At each time step t , the agent applies an action a_t (CIO/bias adjustments) that affects cell selection and handover behavior; the simulator then deterministically and stochastically updates all underlying variables and returns the next observation s_{t+1} . Formally, the Markov property is enforced by constructing the state s_t to summarize all information required to predict the distribution of the next step, including the current serving cell/sector, current load indicators (e.g., PRB utilization), current radio measurements (e.g., RSRP/SINR/CQI statistics), and the current QoS/queue summaries (e.g., packet delay, jitter, loss, throughput aggregates). Given s_t and a_t , s_{t+1} is generated through a sequence of sub-updates: (i) UE mobility updates positions and velocities; (ii) propagation and fading update link gains and instantaneous SINR; (iii) traffic arrivals update per-UE buffers; (iv) the MAC scheduler allocates PRBs and determines served bits, packet departures, and experienced delay; and (v) handover logic updates the serving sector and consequently the spatial distribution of load. Randomness in $P(\cdot)$ comes from mobility perturbations, log-normal shadowing, small-scale fading, and stochastic traffic arrivals, while the remaining steps are governed by the simulator's deterministic rules.

User mobility follows a Gauss–Markov process so that motion is temporally correlated and realistic rather than i.i.d. From the UE position p_t and velocity v_t , the next velocity is sampled as

$$v_{t+1} = \alpha v_t + (1 - \alpha) \bar{v} + \sqrt{1 - \alpha^2} w_t \quad (25)$$

where $\alpha \in (0,1)$ controls memory (higher α yields smoother trajectories), \bar{v} is the nominal drift speed/direction, and w_t is zero-mean Gaussian noise capturing random fluctuations. The position is then updated by $p_{t+1} = p_t + v_{t+1} \Delta T$, with boundary handling (e.g., reflection or wrap-around) applied to keep users inside the simulated area. Given p_{t+1} , propagation is updated by computing the received power from each sector using a distance-dependent path-loss model plus large-scale and small-scale effects. Specifically, the link gain includes path loss $PL(d)$ (e.g., $PL(d) = PL_0 + 10n \log_{10}(d/d_0)$), log-normal shadowing $X_\sigma \sim \mathcal{N}(0, \sigma^2)$ to represent slow obstruction

variations, and Rayleigh fading to model fast multipath. These components determine instantaneous SINR values,

$$\text{SINR}_{u,c}(t+1) = \frac{P_{u,c} G_{u,c}(t+1)}{\sum_{c' \neq c} P_{u,c'} G_{u,c'}(t+1) + N_0} \quad (26)$$

which are mapped to CQI/MCS and achievable spectral efficiency. The agent's action a_t influences association and handovers via CIO-biased cell selection (e.g., RSRP/CQI plus CIO offsets) together with the A3-style event logic (hysteresis and TTT), which determines whether a UE remains with its current sector or transitions to a neighbor. This association update directly changes the per-sector set of active UEs and therefore the next-step load and interference conditions.

Traffic and scheduling complete the transition. For each UE, packet arrivals are generated according to the configured traffic model (e.g., full-buffer for saturated users and Poisson/bursty arrivals for best-effort flows), producing per-UE queue updates $q_{t+1} = \max\{0, q_t + A_t - D_t\}$, where A_t denotes new arrivals and D_t denotes departures served during $[t, t + \Delta T]$. The MAC scheduler assigns PRBs based on current channel quality and QoS urgency (e.g., HOL delay), converting CQI to MCS, translating allocated PRBs into served bits, and updating packet-level metrics such as throughput, HOL delay, jitter, and packet loss (due to deadlines or buffer management). Because scheduling depends on both the instantaneous radio (CQI/SINR) and the number of contending UEs per sector, the association outcome driven by a_t has a second-order effect on latency and reliability through resource contention. The discount factor $\gamma \in (0,1)$ weights near-term QoS and mobility stability more strongly than distant outcomes, reflecting the fast time scale of radio scheduling and handover decisions. With γ close to 1 (e.g., $\gamma = 0.99$), the agent remains sensitive to long-term effects such as persistent congestion and repeated ping-pong events, while still prioritizing immediate QoS improvements; this is crucial because CIO changes can improve short-term throughput but harm long-term stability if they induce excessive handovers or oscillations.

Objective

The control objective is to learn a stationary policy $\pi(a | s)$ that maps the current observed network state s_t to a distribution over admissible control actions a_t (i.e., CIO adjustments), such that the long-term QoS performance is maximized under stochastic mobility, traffic, channel variations, and handover dynamics. Because the environment is inherently random, the objective is defined in expectation over trajectories generated by the interaction of the policy with the transition dynamics \mathcal{P} . Specifically, the optimal policy π^* is obtained by maximizing the expected discounted cumulative reward (return):

$$\pi^* = \arg \max \left(\mathbb{E}_\pi \left[\sum_{t=0}^{\infty} \gamma^t R(s_t, a_t) \right] \right), \quad a_t \sim \pi(\cdot | s_t) \quad (27)$$

The discount factor $\gamma \in (0,1)$ ensures the return remains well-defined and encodes the relative importance of near-term versus long-term outcomes. In our setting, load balancing actions can have delayed effects because changes in CIO influence association and handovers gradually, which then affects PRB utilization, queue evolution, and delay/packet loss over subsequent intervals. We therefore set $\gamma = 0.99$ to place strong emphasis on sustained QoS improvements and stability, rather than short-lived gains that may increase future congestion or trigger excessive handover churn. Although the summation is written over an infinite horizon, in an episodic simulation the effective return is naturally truncated by the episode length; using a high γ still encourages decisions that remain beneficial over the full episode and discourages policies that over-optimize immediate KPIs at the expense of longer-term user experience.

IV. PROPOSED METHOD

We propose a PPO agent that learns to control CIO values dynamically under realistic 5G network conditions. Unlike deterministic value-based approaches such as CDQL, PPO uses a stochastic actor-critic framework with clipped updates, ensuring smooth policy evolution and robustness to noise, user mobility, and non-stationary traffic.

A. Policy and Value Networks

We adopt a stochastic actor-critic parameterization consistent with PPO, in which the actor (policy) produces a *distribution* over continuous CIO control actions and the critic predicts the state value used for advantage estimation. The action at each decision epoch is an M -dimensional vector (one component per BS/sector), so the policy $\pi_\theta(a | s)$ is modeled as a diagonal Gaussian in an unconstrained latent space. Given the current state s_t , the policy network outputs the mean vector $\mu_\theta(s_t) \in \mathbb{R}^M$ and a corresponding element-wise standard deviation $\sigma_\theta(s_t) \in \mathbb{R}_+^M$, defining a factorized normal distribution over an intermediate variable u_t . Sampling is implemented via the reparameterization form

$$u_t = \mu_\theta(s_t) + \sigma_\theta(s_t) \odot \varepsilon_t, \quad \varepsilon_t \sim \mathcal{N}(0, I) \quad (28)$$

which makes the stochasticity explicit through ε_t and enables low-variance gradient estimation during backpropagation. This stochastic policy is important in our setting because the mapping from CIO biases to QoS outcomes is highly non-linear and noisy due to mobility, fast channel fluctuations, and queueing/scheduling effects; maintaining exploration through a

non-degenerate action distribution helps PPO avoid prematurely converging to brittle, locally optimal CIO patterns. Because CIO parameters are operationally bounded (e.g., $[\text{CIO}_{\min}, \text{CIO}_{\max}]$ in dB), the raw Gaussian samples u_t cannot be applied directly. We therefore transform the unconstrained action through a smooth squashing nonlinearity and then map it to the valid CIO range:

$$\hat{a}_t = \tanh(u_t), a_t = \text{scale}(\hat{a}_t, \text{CIO}_{\min}, \text{CIO}_{\max}) \quad (29)$$

The $\tanh(\cdot)$ function guarantees $\hat{a}_t \in (-1, 1)$ component-wise without discontinuous clipping, which is beneficial for stable learning because it preserves smooth gradients and avoids creating large flat regions in the action-to-reward landscape. The scaling operator is a deterministic affine mapping applied per dimension, typically of the form $a_t = \text{CIO}_{\min} + \frac{\hat{a}_t + 1}{2} (\text{CIO}_{\max} - \text{CIO}_{\min})$, so that $\hat{a}_t = -1$ corresponds exactly to CIO_{\min} and $\hat{a}_t = +1$ corresponds to CIO_{\max} . In the PPO update, the likelihood $\pi_{\theta}(a_t | s_t)$ required for the probability ratio can be evaluated consistently by computing the Gaussian log-density in the pre-squash space and accounting for the tanh transformation through the standard change-of-variables term, ensuring that the clipped surrogate objective reflects the true bounded-action policy.

The critic is implemented as a separate value network $V_{\psi}(s_t)$ that approximates the expected discounted return from the current state under the current policy, $V_{\psi}(s_t) \approx \mathbb{E}_{\pi}[\sum_{k \geq 0} \gamma^k r_{t+k} | s_t]$. This estimate serves as a baseline to reduce variance in policy-gradient learning and is used directly in the Generalized Advantage Estimation recursion that follows in the next subsection. Since QoS improvements and mobility effects can be delayed (e.g., CIO changes may only translate into different associations after handover conditions are met and queues respond), the value function is essential for assigning credit over time rather than reacting only to instantaneous KPI fluctuations.

Both actor and critic are realized as lightweight feedforward multilayer perceptrons to keep inference compatible with near-real-time control loops. The input to each network is the normalized observation vector (per-cell aggregates and mobility/QoS summaries after filtering/normalization), and the networks use ReLU activations in 2–3 hidden layers with widths in the 128–256 range; in our default configuration we employ a two-layer 256 – 256 MLP for both policy and value heads. The policy output layer produces an M -dimensional mean and an M -dimensional dispersion parameter (commonly implemented as $\log \sigma_{\theta}(s_t)$ passed through an exponential or softplus to ensure positivity), while the value network outputs a single scalar. To prevent pathological exploration behavior during training, it is standard to bound the predicted log-variance to a reasonable interval (avoiding vanishing

exploration or excessively noisy actions), which improves numerical stability when computing PPO likelihood ratios and entropy regularization under noisy observations.

B. Advantage Estimation

Policy-gradient methods require an estimate of how much better (or worse) a selected action was compared to the policy's typical performance in the same state. This quantity is captured by the advantage function $A^{\pi}(s_t, a_t) = Q^{\pi}(s_t, a_t) - V^{\pi}(s_t)$, which measures the relative benefit of taking a_t in s_t rather than acting according to the policy's average behavior. In practice, directly estimating Q^{π} is noisy in stochastic environments such as mobile 5G systems, where rewards depend on coupled effects of mobility, fading, queueing, and handovers. Using high-variance advantage estimates often leads to unstable updates and slow convergence, especially when observations are noisy or delayed. To obtain a stable and sample-efficient learning signal, we employ Generalized Advantage Estimation (GAE), which constructs a smoothed multi-step advantage estimate by combining temporal-difference residuals across multiple horizons.

We first compute the one-step temporal-difference (TD) error, which quantifies the instantaneous surprise between the observed reward plus the critic's estimate of the next state value and the critic's estimate of the current state value:

$$\delta_t = r_t + \gamma V_{\psi}(s_{t+1}) - V_{\psi}(s_t) \quad (30)$$

In this expression, r_t is the reward obtained after applying the CIO action at time t , and $V_{\psi}(\cdot)$ is the value network's approximation of the expected discounted return. The TD error can be interpreted as a local estimate of advantage: if δ_t is positive, the realized outcome was better than what the critic predicted for state s_t ; if it is negative, the outcome was worse. However, a purely one-step estimate is often too noisy because the impact of load balancing decisions can manifest over several subsequent steps, for example when CIO changes gradually shift associations and queues respond with delay. For this reason, we accumulate information over multiple steps. GAE forms an exponentially weighted sum of these TD errors, producing an advantage estimate that interpolates between high-variance, low-bias Monte Carlo returns and low-variance, higher-bias one-step TD estimates:

$$\hat{A}_t = \sum_{l=0}^{T-1-t} (\gamma \lambda)^l \delta_{t+l} \quad (31)$$

Here, T denotes the rollout horizon (or episode truncation point), and $\lambda \in [0, 1]$ governs the bias–variance trade-off. When λ is close to one, the estimator incorporates longer-horizon information and becomes closer to a Monte Carlo-style

advantage, which better captures delayed effects but can increase variance. When λ is close to zero, the estimator approaches the one-step TD residual δ_t , yielding lower variance but potentially under-crediting actions whose benefits appear later. In QoS-aware load balancing, where the effects of a CIO adjustment may unfold over several control intervals, choosing λ near one typically improves credit assignment without requiring very long rollouts; a common and effective choice is $\lambda = 0.95$, which we adopt to emphasize medium-term QoS evolution while maintaining stable learning.

The same construction provides a consistent target for training the value network. Specifically, we define the bootstrapped return target for the critic as

$$\hat{V}_t^{\text{tgt}} = \hat{A}_t + V_\psi(s_t) \quad (32)$$

which corresponds to an estimate of the state return that combines the critic's baseline with the multi-step advantage correction. Using \hat{V}_t^{tgt} as the regression target aligns the critic with the policy's observed rollouts while still leveraging bootstrapping through $V_\psi(s_{t+1})$. This is particularly important in our setting because observation noise and mobility-driven nonstationarity can make pure Monte Carlo targets unnecessarily noisy; the bootstrapped GAE target improves stability and typically reduces sensitivity to stochastic fluctuations in channel and traffic realizations.

C. Clipped Surrogate Objective

Let the probability ratio be:

$$r_t(\theta) = \frac{\pi_\theta(a_t|s_t)}{\pi_{\theta_{\text{old}}}(a_t|s_t)} \quad (33)$$

The clipped objective used to update the policy is:

$$L^{\text{clip}}(\theta) = \mathbb{E}_t[\min(r_t(\theta)\hat{A}_t, \text{clip}(r_t(\theta), 1 - \epsilon, 1 + \epsilon)\hat{A}_t)] \quad (34)$$

To encourage exploration, we add an entropy bonus:

$$L^{\text{ENT}}(\theta) = \mathbb{E}_t[H(\pi_\theta(\cdot|s_t))] \quad (35)$$

and to stabilize value predictions, a value loss:

$$L^V(\psi) = \mathbb{E}_t[(V_\psi(s_t) - \hat{V}_t^{\text{tgt}})^2] \quad (36)$$

The combined PPO objective is:

$$\max_{\theta, \psi} L^{\text{clip}}(\theta) + c_{\text{ent}} L^{\text{ENT}}(\theta) - c_v L^V(\psi) \quad (37)$$

where c_{ent} and c_v balance exploration and value accuracy.

D. Reward Normalization and Stability

Because our reward is a weighted combination of heterogeneous KPIs (throughput, fairness, latency, jitter, packet-loss ratio, and handovers), the raw terms naturally live on very different numerical scales and exhibit different distribution shapes. Throughput is typically bounded but can vary widely with channel and scheduling; fairness (e.g., Jain's index) is constrained to $[0, 1]$; latency, jitter, and PLR often have *heavy tails* (rare congestion episodes can produce extremely large values); and handovers are event-driven counts that appear as sparse spikes. If these signals are combined without careful normalization, the learning signal becomes dominated by whichever KPI has the largest magnitude or most extreme outliers, which can destabilize advantage estimates and lead to oscillatory policies that chase transient anomalies rather than improving sustained QoS. For this reason, we explicitly normalize and stabilize each KPI contribution before forming the scalar reward.

We first map each KPI term into a comparable $[0, 1]$ range using running statistics computed online. The goal is to ensure that a meaningful improvement in any KPI produces a reward change of similar order, so that the chosen weights w_k reflect actual preference rather than compensating for unit mismatches. In practice, we maintain streaming estimates of central tendency and spread (e.g., running mean/variance or running percentiles) for each KPI channel over a recent window of interactions, and we normalize the current measurement relative to those statistics before applying the reward weights. This procedure is applied consistently at the control sampling interval ΔT , matching how KPIs are collected and stacked into the state and reward terms in the simulator.

A second normalization step is required because not all KPIs have the same direction. Throughput and fairness are higher-is-better, while latency, jitter, PLR, and handovers are lower-is-better in our formulation. To make the reward composition consistent, we convert every normalized KPI into a common orientation so that larger values always correspond to better performance. Concretely, for lower-is-better metrics we apply an inversion after normalization (or equivalently normalize the negative quantity), so that reduced delay/jitter/loss and fewer handovers contribute positively in the unified $[0, 1]$ scale. This makes the subsequent scalarization in the reward function behave predictably: increasing any goodness term always increases reward, and the weights w_k can be interpreted directly as preference parameters over comparable dimensions.

Latency, jitter, and PLR are particularly prone to rare but extreme outliers caused by transient overload, bursts, or mobility-triggered disruptions. If these outliers enter the reward linearly, they can overwhelm the learning signal and cause unstable policy updates, especially under PPO where the

advantage magnitude influences the gradient direction even with clipping. To mitigate this, we apply a saturating nonlinearity—implemented as a sigmoid-style clipping—to these channels before they are combined into the reward. Intuitively, once latency or PLR exceeds a “severe” operating region (often aligned with an SLA-like threshold or a high percentile of recent history), further increases should not keep scaling the penalty proportionally, because doing so would force the agent to overreact to a small number of catastrophic samples. The sigmoid transformation compresses the tails, preserving sensitivity around the normal operating regime (where incremental improvements matter) while suppressing extreme values that would otherwise dominate training.

Handover-related penalties present a different stability issue: handovers occur as discrete events and therefore introduce high-variance reward spikes. Penalizing the raw per-step handover count can make the policy overly conservative, discouraging even beneficial transitions that relieve congestion, or can lead to thrashing if the agent learns to react to short-lived measurement fluctuations near cell borders. To address this, we smooth the handover penalty using an exponential moving average, effectively turning sparse event spikes into a continuous estimate of recent handover rate. This discourages persistent churn (including ping-pong patterns) while still allowing legitimate handovers when the longer-term payoff is sustained, which aligns with our goal of balancing mobility stability and congestion relief under A3-style handover dynamics and ping-pong definitions.

Finally, even with stabilized KPI terms, the controller can still exhibit undesirable actuation instability by changing CIO values too aggressively from one control interval to the next. Such rapid CIO swings can create oscillatory association decisions around overlap regions, which increases signaling, perturbs queues, and amplifies jitter—effects that are especially harmful under noisy observations. We therefore add an explicit smoothness regularizer that penalizes large step-to-step changes in the action vector:

$$R_s(t) = -\frac{\|a_t - a_{t-1}\|_2^2}{\Delta_a^2} \quad (38)$$

This term is a quadratic penalty on the rate of change of the CIO control signal (analogous to control-theoretic input-slew regularization). The normalization factor Δ_a^2 sets the scale of acceptable CIO variation per interval; changes much smaller than Δ_a incur only mild penalty, whereas abrupt multi-dB jumps are strongly discouraged. In effect, the agent is encouraged to implement offloading as a sequence of small, consistent nudges rather than sudden reversals, which reduces ping-pong propensity and improves temporal consistency of QoS. Our ablations also reflect this behavior: removing the smoothness term increases volatility and weakens stability-related metrics,

confirming that this regularizer is not cosmetic but directly shapes a calmer, more deployable control policy.

E. Training Procedure

The training of the PPO agent was carried out entirely in Python using a custom-built simulator that reproduces network behavior, user mobility, and QoS dynamics. The process follows an iterative structure where, in each training cycle, the agent interacts with the simulated environment, evaluates its performance, and updates its policy to improve future decisions. Each training iteration begins with the rollout phase, during which the current policy interacts with the environment for a fixed number of steps. At every step, the agent observes the current network state—such as throughput, latency, jitter, and handover activity—selects an action representing new CIO values, and applies it to the environment. The simulator then updates the network condition and returns a corresponding reward that reflects how well the new configuration balanced the load and improved overall QoS. These experiences are collected and stored for later updates. After completing a rollout, the advantage estimation phase evaluates how much better each action performed compared to the agent’s previous expectations. This comparison helps the agent identify which decisions were beneficial and which were not, allowing it to focus future learning on actions that consistently lead to performance improvements. Next, during the optimization phase, the stored data is divided into mini-batches, and the neural networks representing the policy (actor) and the value function (critic) are updated over several passes. The updates are designed to make gradual improvements rather than aggressive policy changes, ensuring the learning process remains stable. The optimization combines three objectives: maximizing expected performance, improving value prediction accuracy, and maintaining enough randomness in actions to encourage exploration. Finally, stability controls are applied to prevent overfitting or sudden policy divergence. These include limiting large policy changes between updates, clipping gradients to keep them within a safe range, and normalizing the collected data so that each batch contributes evenly to learning. Training continues for multiple iterations until the cumulative reward and QoS metrics—such as throughput and latency—converge to stable values. Over time, the PPO agent learns an effective CIO adjustment policy that intelligently balances network load, minimizes handovers, and enhances the overall service quality across dynamic and noisy network conditions.

F. Advantages of PPO in 5G Load Balancing

The adoption of the PPO algorithm offers several distinct advantages for dynamic load balancing and mobility management in 5G networks.

First, PPO provides smooth and adaptive control over CIO values. Since it operates with continuous actions and applies a

clipping mechanism to limit drastic policy updates, the algorithm avoids abrupt changes that could cause ping-pong handovers or instability in user association. This smooth adjustment behavior is particularly beneficial in fast-changing radio environments, where small, consistent corrections yield more stable and reliable handover performance.

Second, PPO ensures stable and efficient learning under the noisy and partially observable conditions typical of real-world cellular systems. The combination of clipped policy updates and advantage estimation helps the training process remain robust, even when the feedback data contains uncertainty or short-term fluctuations. This stability allows the agent to maintain steady progress without overreacting to transient measurement noise or irregular user movement patterns.

Third, PPO naturally supports multi-objective optimization, making it well suited for problems that involve multiple conflicting KPIs. By designing a weighted reward structure, the agent can dynamically balance trade-offs among throughput, latency, jitter, fairness, packet loss, and handover rate. This capability allows network operators to prioritize specific objectives—such as reducing latency during congestion or improving fairness under uneven load—without retraining the entire model.

Finally, PPO demonstrates strong robustness and generalization capabilities. Its stochastic policy formulation enables the agent to explore a variety of CIO configurations and adapt to new network conditions, user mobility patterns, and traffic distributions more effectively than deterministic reinforcement learning algorithms. As a result, the PPO-based framework achieves a more flexible and resilient performance, maintaining high QoS across diverse and unpredictable 5G environments.

G. Objective Summary

The ultimate goal of the proposed PPO-based agent is to learn a control policy that continuously adjusts the Cell Individual Offset (CIO) values to maximize long-term network performance. Rather than optimizing for a single metric, the agent is trained to improve a weighted combination of several key performance indicators, including throughput, jitter, packet loss ratio, latency, fairness, and handover rate.

Through continuous interaction with the simulated environment, the policy learns how different CIO configurations influence user association, network load distribution, and overall service quality. By optimizing the cumulative reward over time, the agent gradually develops the ability to balance multiple objectives simultaneously—enhancing throughput and fairness while minimizing latency, packet loss, and unnecessary handovers.

Once trained, the learned policy operates as an intelligent decision-making mechanism that autonomously adapts to varying network conditions, user mobility, and traffic patterns. This allows the system to maintain high-quality connectivity

and efficient resource utilization in dynamic 5G environments. In essence, the PPO agent acts as a self-optimizing controller that continuously fine-tunes the network toward an equilibrium state where overall QoS is maximized and performance trade-offs are managed effectively.

V. PERFORMANCE EVALUATION

We optimize a multi-objective reward that balances six QoS/control KPIs with an action-smoothness regularizer:

$$r_t = \sum_{k \in \mathcal{K}} w_k \hat{x}_{k,t} - \lambda_s \| a_t - a_{t-1} \|_2 \quad (39)$$

where $\mathcal{K} = \{\text{thr, fair, lat, jit, plr, ho}\}$ and Each KPI is normalized to $[0,1]$ with directionality encoded:

$$\hat{x}_{k,t} = \begin{cases} \text{clip}\left(\frac{x_{k,t} - m_k}{M_k - m_k}, 0, 1\right), & \text{higher is better} \\ \text{clip}\left(\frac{M_k - x_{k,t}}{M_k - m_k}, 0, 1\right), & \text{lower is better} \end{cases} \quad (40)$$

where m_k, M_k are the 5th/95th percentiles of $x_{k,t}$ measured on a held-out validation set (to avoid reward drift and outlier domination). We treat throughput (thr) and fairness (fair) as higher-is-better; latency (lat), jitter (jit), packet-loss ratio (plr), and handovers (ho) as lower-is-better. The action a_t is the per-cell CIO adjustment vector; λ_s penalizes rapid changes to discourage ping-pong.

We chose the reward weights w_k using a reproducible two-stage procedure that turns the multi-KPI design into a single, well-defined selection rule. Let $m(w)$ denote the KPI summary vector obtained after training and evaluation with a candidate weight vector $w = \{w_{\text{thr}}, w_{\text{fair}}, w_{\text{lat}}, w_{\text{plr}}, w_{\text{jit}}, w_{\text{ho}}\}$. Because these KPIs have different units and good directions, we first map each KPI to a dimensionless, bounded score so that weighting is meaningful. For each KPI k , we compute a normalized utility $\tilde{u}_k \in [0,1]$ where larger is better. For beneficial metrics such as throughput and fairness we use $\tilde{u}_k = \text{clip}\left(\frac{x_k - x_k^{\min}}{x_k^{\max} - x_k^{\min}}, 0, 1\right)$, while for cost metrics such as latency, PLR, jitter, and handovers we invert the scale using $\tilde{u}_k = 1 - \text{clip}\left(\frac{x_k - x_k^{\min}}{x_k^{\max} - x_k^{\min}}, 0, 1\right)$. The per-step reward then follows the scalarization used in the paper: $r_t(w) = \sum_k w_k \tilde{u}_k(t) - \lambda_s \| a_t - a_{t-1} \|_2^2$, where a_t is the CIO action at step t and the smoothness term discourages oscillatory control (which otherwise appears as ping-pong behavior and jitter spikes).

With this consistent reward definition, we performed a coarse search over the weight simplex by enumerating candidate weight vectors on a grid (e.g., a simplex grid with step Δ such as 0.05 or 0.1, constrained by $\sum_k w_k = 1$ and $w_k \geq 0$). For each candidate w , we trained PPO under the same training budget

and evaluated it over multiple independent runs (seeds) to obtain stable KPI summaries $m(w)$, computed as averages over the evaluation horizon (and, if you report tail metrics, over the chosen percentile). We then enforced the SLA-like constraints as a hard feasibility filter: a candidate w is feasible if $\text{lat}(w) \leq 25$ ms and $\text{PLR}(w) \leq 5\%$, where $\text{lat}(w)$ and $\text{PLR}(w)$ are measured. This feasibility screen is important because it prevents selecting weightings that artificially inflate throughput by tolerating unacceptable queueing delay or packet loss.

Among the feasible candidates, we applied a Pareto screen to avoid picking a solution that is strictly worse across the KPI set. Concretely, after converting KPIs to higher-is-better normalized utilities, we say that w_1 dominates w_2 if $\tilde{u}_k(w_1) \geq \tilde{u}_k(w_2)$ for all k and $\tilde{u}_j(w_1) > \tilde{u}_j(w_2)$ for at least one KPI j . We keep only the non-dominated set \mathcal{P} . To choose a single operating point from \mathcal{P} in a way that is objective and repeatable, we selected the balanced knee by minimizing the distance to an ideal point in normalized KPI space: $w^* = \arg \min_{w \in \mathcal{P}} \| \tilde{u}^{\text{ideal}} - \tilde{u}(w) \|_2$, where \tilde{u}^{ideal} is the componentwise best utility observed among feasible candidates, i.e., $\tilde{u}_k^{\text{ideal}} = \max_{w \in \mathcal{P}} \tilde{u}_k(w)$. This rule tends to select a policy that is close to the best-achievable values across all KPIs without over-optimizing a single metric, and it makes the weight choice defensible: it is not hand-picked, it is the result of a defined constrained search plus a standard multi-objective selection criterion.

The resulting weights are included in table 1. This distribution reflects two practical observations from the feasibility and Pareto screens. First, throughput and latency must be emphasized to keep capacity high while preventing queue build-up, and PLR must be controlled but typically becomes critical only when latency has already deteriorated under overload, so it can receive a moderate weight once the SLA filter is enforced. Second, fairness meaningfully reduces utilization skew (which otherwise creates persistent hot cells and worsens tail latency), so it is weighted comparably to latency rather than treated as an afterthought. The handover weight is intentionally small because stability is primarily achieved through the smoothness regularization term $\lambda_s \| a_t - a_{t-1} \|_2^2$ and because over-penalizing handovers can trap UEs in overloaded cells and increase delay/loss when congestion relief requires a controlled mobility response. In other words, the design discourages needless mobility churn without preventing legitimate handovers that improve system-level QoS.

Finally, to demonstrate that the reported gains are not fragile to preference specification, we include controlled sensitivity checks that modify one component at a time while keeping the rest fixed: uniform weights $w_k = 1/6$ to test the benefit of preference shaping; removing fairness by setting $w_{\text{fair}} = 0$ to quantify its impact on utilization skew and tail delay; doubling the handover penalty to illustrate the trade-off between mobility

stability and congestion relief; setting $\lambda_s = 0$ to expose oscillatory CIO behavior and its effect on jitter/ping-pong; and perturbing each weight by $\pm 50\%$ one at a time to produce spider/radar summaries of KPI robustness. If you want this to be fully airtight for reviewers, add one sentence stating whether you renormalize weights after perturbation and one sentence specifying whether latency/PLR constraints are applied to the mean or a chosen percentile over the evaluation window.

Table 1. The final weights

w_{thr}	w_{fair}	w_{lat}	w_{plr}	w_{jit}	w_{ho}
0.35	0.20	0.20	0.1	0.1	0.05

We measure cell-level fairness using Jain's index:

$$J = \frac{(\sum_{i=1}^n x_i)^2}{n \sum_{i=1}^n x_i^2}, \quad J \in \left[\frac{1}{n}, 1 \right] \quad (41)$$

where x_i is the per-cell served rate (cell-aggregate downlink throughput averaged over the evaluation window).

To substantiate robustness, we introduce controlled perturbations on observations and mobility and report KPI degradation curves and confidence intervals:

- Measurement noise: RSRP noise $\sigma_{\text{RSRP}} \in \{1, 3, 5\}$ dB; CQI noise $\sigma_{\text{CQI}} \in \{0.5, 1, 2\}$; latency/jitter noise $\sigma \in \{2, 5, 10\}$ ms (added i.i.d. to reports).
- Reporting delay & loss: observation lag $L \in \{0, 100, 200, 500\}$ ms via FIFO; missingness $p_{\text{miss}} \in \{0, 1, 5, 10\}\%$ with zero-order hold imputation.
- Mobility regimes: pedestrian (1.5 m/s), urban vehicular (15 m/s), and highway (30 m/s); turning dynamics from the Gauss–Markov α sweep $\{0.2, 0.6, 0.9\}$.

We provide robustness plots for each KPI vs. σ , L , p_{miss} , and speed, and report tail metrics (95th/99th latency), HO failure, and session interruption rates. PPO maintains the best KPI trade-off under strong perturbations; off-policy baselines degrade more under lag/missingness, consistent with their reliance on older replay.

Beyond the tri-sector macro layout, we evaluate generalization across larger macro networks—including a 7-site hexagonal deployment and a 19-site variant—as well as macro networks augmented with small-cell overlays in which pico cells are Poisson-distributed with an inter-site distance of approximately 200 m. Traffic heterogeneity is captured by a mix of full-buffer, web-browsing, and video flows (CBR and ON–OFF patterns) shaped by a diurnal profile. We also sweep the CIO control interval ΔT over $\{0.5, 1, 5\}$ s to test sensitivity to actuation frequency. To assess transfer, we train on one topology and UE-density setting and evaluate zero-shot on held-out topologies/densities before allowing limited fine-tuning. We

report zero-shot performance and fine-tuning sample complexity, measured as the number of episodes needed to reach 95% of the trained-policy KPI. Across these settings, PPO generalizes best over site counts and maintains higher fairness at comparable throughput. The MAC scheduler is weighted proportional fair (W-PF) with delay awareness:

$$\text{score}_u = \left(\frac{R_{u,t}}{\bar{R}_{u,t}} \right)^{1-\beta} \cdot \left(\frac{\text{HOL}_{u,t}}{\bar{\text{HOL}}_t} \right)^\beta \cdot w_{\text{QCI}}(u) \quad (42)$$

where $R_{u,t}$ is the instantaneous rate estimate, $\bar{R}_{u,t}$ its exponential average, $\text{HOL}_{u,t}$ the head-of-line delay, and w_{QCI} a per-class weight. We model HARQ with up to 4 processes and RLC-AM buffering; CQI drives MCS selection with standard BLER targeting. Handover outcomes follow 3GPP-aligned definitions:

- HO failure rate: fraction of HOs where RLF occurs within T_{HOF} after HO command.
- Ping-pong rate: fraction of HOs returning to the source cell within T_{PP} (we use $T_{\text{PP}} = 5\text{s}$). We report both alongside HO counts. PPO reduces HO failures and ping-pong relative to all baselines, particularly at vehicular speeds.

Figures 2–4 set up the operating conditions and why the control problem is non-trivial. Figure 2 plots the SINR field over a $1000 \times 1000 \text{ m}$ area with three base stations and overlays a representative UE path that deliberately traverses overlapping coverage seams.

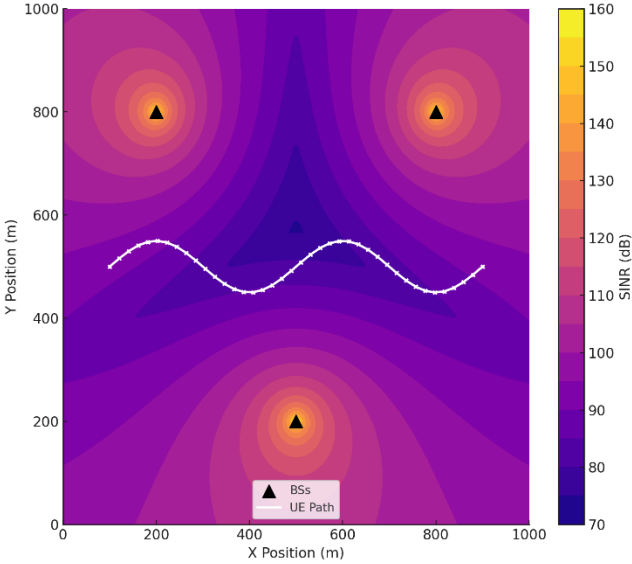


Figure 2. SINR Zones with UE Path.

The bright regions are strong, the darker regions are interference-limited. This visual makes clear that a “strongest-signal” decision alone is insufficient: as the path cuts through overlap, small CIO nudges can reassign a UE, and the right

decision must weigh radio quality and instantaneous load to avoid creating or sustaining congestion. The path selection here is important: it repeatedly challenges the controller at ambiguous borders where load-aware association can deliver outsized gains in delay and loss, despite modest radio penalties. Figure 3 illustrates a spatial received-power heatmap over a $1 \text{ km} \times 1 \text{ km}$ area that combines large-scale and small-scale propagation effects in one view. For every location on the grid, the received power is computed by starting from a sector’s transmit power and antenna gain, then subtracting the distance-dependent path loss (signal decays with distance from each base station), adding a log-normal shadowing term to represent slow variations caused by obstacles and local clutter (creating broad patches where coverage is better/worse than pure distance would predict), and finally adding Rayleigh fading to capture fast multipath fluctuations (responsible for the finer grain/noisy texture on top of the shadowing field). The heatmap value at each point is the best-serving (strongest) sector among all sectors, so the map naturally forms coverage regions and transition zones between cells. On top of the heatmap, the base-station sites are shown with triangle markers, and the UE trajectory is plotted as a continuous line to show how the user moves through different coverage conditions. As the UE crosses areas where another sector becomes sufficiently stronger than the current serving sector, handover events are triggered, using a standard A3-style decision logic with hysteresis and a TTT so that handovers occur only when the advantage is sustained rather than caused by momentary fading spikes.

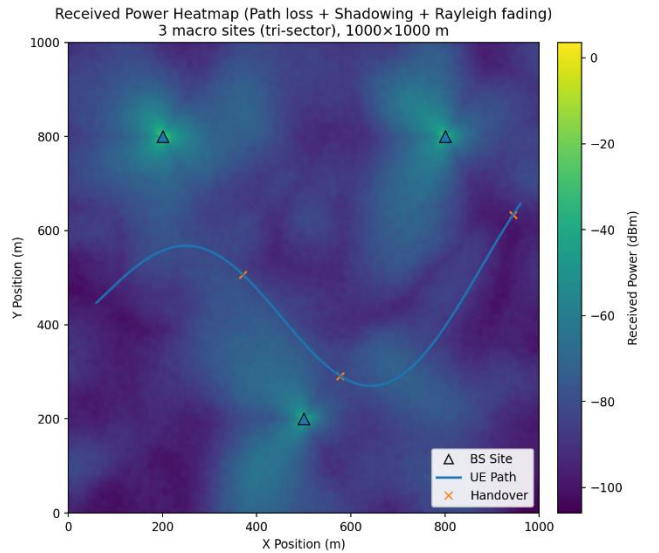


Figure 3. Received-power heatmap over a $1000 \times 1000 \text{ m}$ area, combining distance-based path loss, log-normal shadowing ($\sigma = 6 \text{ dB}$), and Rayleigh small-scale fading. The UE trajectory and handover locations are overlaid; BS sites are marked by triangles..

Overall, this plot is useful because it visually demonstrates why coverage and handover behavior are not perfectly smooth: even

at the same distance from a base station, shadowing and multipath can create realistic local variations that affect serving-cell selection and handover locations. Early in learning, frequent handovers are expected as the policy explores the action space; with training, the controller should switch only when a persistent benefit is detectable (relief of queueing, reduction in loss or jitter), not on the basis of momentary RSRP/CQI spikes. The intent of figure 3 is to demonstrate that the agent’s learned CIO adjustments become small, smooth, and selective rather than reactive.

Table 2. Simulation Environment Configuration

Parameter	Value
Layout / Area	3 macro BS (tri-sector) in a 1000×1000 m area
Carrier Bandwidth (NR)	20 MHz (downlink)
PRBs per BS	106 PRBs (NR, 15 kHz SCS)
Propagation	Path loss + log-normal shadowing ($\sigma = 6 \text{ dB}$) + Rayleigh small-scale fading
Scheduler	QoS-aware MAC (HOL delay and CQI weighted)
Traffic Model	Mixed: full-buffer + Poisson bursty flows
UE Count	45 (swept in scalability experiments)
Mobility Model	Gauss–Markov: $\alpha = 0.90$, $\Delta t = 0.1 \text{ s}$, $E[\text{speed}] = 1.5 \text{ m/s}$, $\sigma = 0.5 \text{ m/s}$
Observation Noise	RSRP $\sigma = 1.0 \text{ dB}$, CQI $\sigma = 0.5$, Latency $\sigma = 2 \text{ ms}$ (Gaussian)
Decision Interval (ΔT)	1.0 s
Episode Length	600 s (600 control steps)
CIO Bounds	$[-6 \text{ dB}, +6 \text{ dB}]$ (per cell)
Handover Definition	3GPP-like A3 with hysteresis & TTT; ping-pong if return $< 5 \text{ s}$
KPI Sampling	Every ΔT ; normalized to $[0,1]$ for reward terms
Simulator Toolchain	Pure-Python custom environment

Table 2 summarizes the default scenario used in all experiments unless stated otherwise: a tri-sector macro deployment over a 1000×1000 m area with 20 MHz NR downlink and 106 PRBs per BS. Traffic combines full-buffer and bursty Poisson flows, and a QoS-aware scheduler prioritizes HOL delay alongside CQI. User mobility follows a Gauss–Markov model ($\alpha = 0.9$; $1.5 \pm 0.5 \frac{m}{s}$), and we inject Gaussian observation noise on RSRP, CQI, and latency to reflect measurement uncertainty. The controller acts every $\Delta T = 1 \text{ s}$ over 600 s episodes, with per-cell CIO constrained to $[-6, +6] \text{ dB}$. Handover follows a 3GPP-like A3 rule, and quick returns ($< 5 \text{ s}$) are counted as ping-pong. All KPIs are sampled every control step and normalized to $[0,1]$ for reward shaping; UE count is 45 by default and is swept in scalability tests.

Table 3 lists the policy and training hyperparameters for PPO that yielded stable learning under mobility and noisy observations. We use $\gamma = 0.99$, $\lambda_{GAE} = 0.95$, and a clip range $\epsilon = 0.2$ with an entropy coefficient of 0.01 and value-loss coefficient 0.5. Optimization uses Adam ($lr = 3e-4$), batch size 64, 8 minibatches, 10 epochs per update, horizon $T=2048$, and max grad-norm 0.5. The actor-critic is an MLP (256–256, ReLU); observations are normalized online, actions are tanh-squashed then scaled to the CIO bounds, and a smoothness penalty ($0.10 \times \|\Delta CIO\|_2$) discourages abrupt bias changes.

Table 3. PPO Hyperparameters (Policy and Training)

Hyperparameter	Value
Discount (γ)	0.99
GAE (λ)	0.95
Clip Range (ϵ)	0.20
Entropy Coefficient	0.01
Value Loss Coefficient	0.50
Learning Rate	$3e-4$
Batch Size (per update)	64
Minibatches	8
Optimization Epochs	10 per update
Rollout Horizon (T)	2048 steps
Max Grad-Norm	0.5
Policy/Value Network	MLP 256–256 (ReLU)
Obs Normalization	Running mean/variance
Action Squash	tanh, then scaled to CIO bounds
CIO Smoothness Penalty	$0.10 \times \ \Delta CIO\ _2$
KL Target / Early Stop	0.01 (early stop if exceeded)
Reward Weights	$w = [+THR, -LAT, -JIT, -PLR, +FAI, -HO]$ (normalized)

Figure 4 illustrates how the PPO agent’s critic and actor behave over a representative 2D slice of the RL state space, where the x-axis is normalized cell load/utilization (e.g., PRB usage) and the y-axis is normalized signal quality (a summary of CQI/RSRP/SINR). The colored heatmap shows the critic value $V_\psi(s)$, i.e., the critic’s estimate of the expected discounted return from each state; brighter regions indicate states expected to yield higher long-term reward under the current policy (typically stronger radio conditions and manageable load), while darker regions correspond to states with lower predicted return (often congested cells and/or weak radio conditions that degrade QoS and increase instability). The overlaid arrows visualize the actor’s mean action $\mu_\theta(s)$ on the same state slice,

interpreted as the policy’s preferred CIO adjustment direction and magnitude: arrows pointing to the right indicate a tendency toward positive CIO (making the sector more attractive, retaining/attracting UEs), while arrows pointing left indicate a tendency toward negative CIO (making the sector less attractive, offloading UEs to neighbors); arrow length reflects the strength of this preference, with saturation consistent with bounded CIO constraints (e.g., $[-6, +6]$ dB). Finally, the semi-transparent scatter points represent visited rollout states sampled during simulation, showing where the system actually operates most of the time (e.g., common mid-load and variable-quality regimes). Overall, the figure provides an intuitive, interpretable view of learned behavior: the critic assigns higher value to favorable load–radio conditions, and the actor pushes the system away from low-value regions (congestion/poor signal) and toward higher-value operating points by adjusting CIO biases that indirectly shape association and handover decisions.

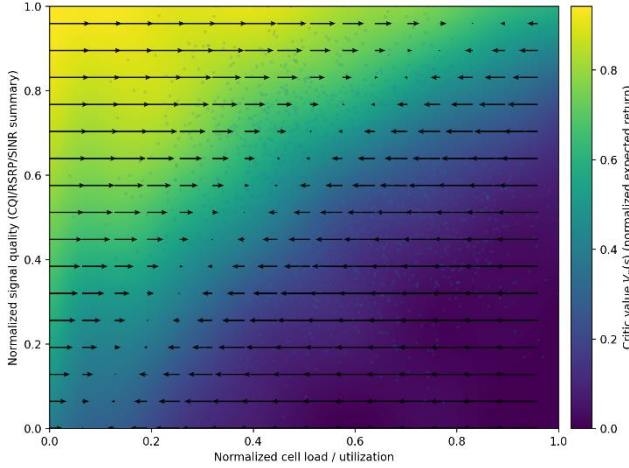


Figure 4. Actor–critic visualization on a 2D state slice (PPO CIO control).

Figures 5–10 trace how the PPO policy improves each KPI over training. In Figure 5, handover counts fall from an exploratory peak to a stable floor, indicating that the controller has learned to suppress oscillatory association and to reserve handovers for cases with sustained payoff (e.g., when offloading prevents a cell from tipping into queue buildup). That reduction in churn supports the monotone improvements in the remaining KPIs. Figure 6 shows Jain’s fairness climbing toward unity and then holding: the policy systematically equalizes offered load across the three sectors, so no single BS accumulates the long queues that drive poor tail latency and elevated drop rates. Figure 7 shows latency dropping and then stabilizing as the scheduler faces fewer hot spots and fewer mid-flow interruptions from unnecessary switches; the end-state delay reflects steady queues consistent with balanced utilization. Figure 8 shows aggregate throughput rising and consolidating around the ~episode-200 mark: balanced load keeps more UEs schedulable at healthier

effective rates and avoids airtime waste from drops and jitter spikes, so the total data delivered per unit time increases even without explicit power control.

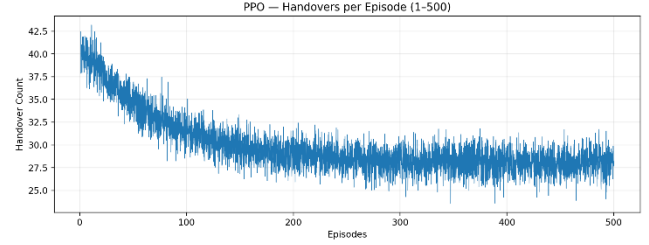


Figure 5. Handover count per episode (training time series).

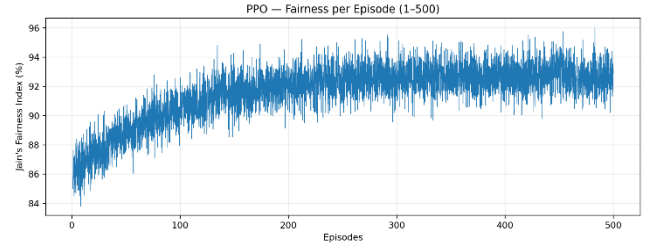


Figure 6. Jain’s fairness index per episode (training time series).

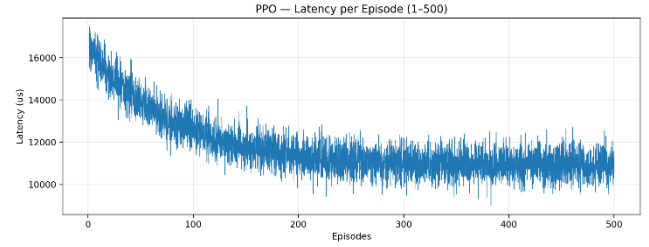


Figure 7. Average latency per episode (training time series).

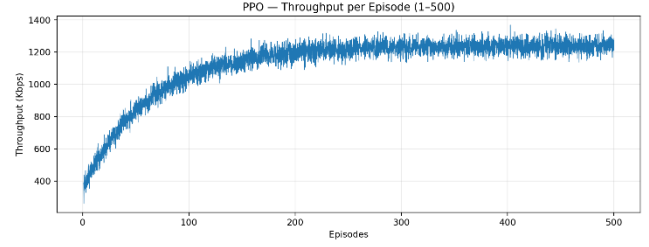


Figure 8. Aggregate throughput per episode (training time series).

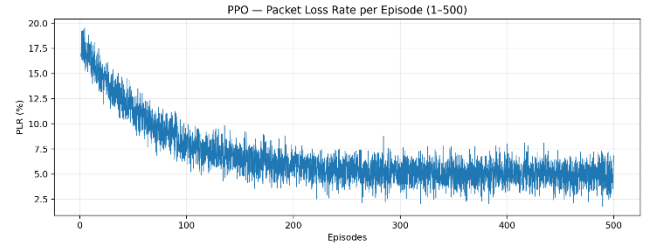


Figure 9. Packet-loss ratio per episode (training time series).

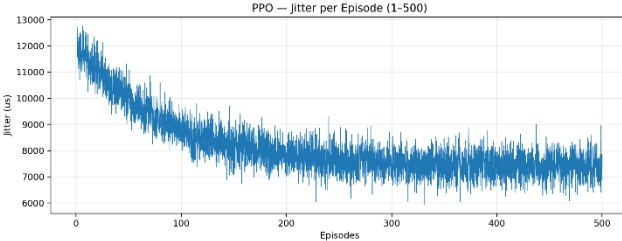


Figure 10. Jitter per episode (training time series).

Figure 9 shows PLR falling as buffers stop overflowing and as flow interruptions become rare; fewer retransmissions also indirectly preserve throughput. Figure 10 shows jitter declining over episodes as the agent “calms” inter-packet timing by avoiding sudden association changes and by preventing short-lived congestion surges.

Experimental protocol and statistical analysis. To ensure statistical reliability, each algorithm is trained using $N = 10$ independent random seeds. Each seed controls the policy network initialization, minibatch shuffling, and stochastic elements of the environment (e.g., fading/shadowing realizations, mobility trace selection, and observation noise). After training, we freeze the learned policy and evaluate it on a shared evaluation set consisting of identical mobility traces and channel/noise seeds across all methods, enabling paired comparisons.

For each KPI (e.g., throughput, packet delay, handover rate, ping-pong rate, RLF rate, and load imbalance), we report the mean, standard deviation, and 95% confidence intervals across seeds. Confidence intervals are computed using a nonparametric bootstrap over seeds (10,000 resamples) or, equivalently, using the t-distribution when appropriate. To quantify whether improvements are statistically significant, we apply a paired Wilcoxon signed-rank test between the proposed method and each baseline on the per-seed KPI values, and correct for multiple comparisons using Holm–Bonferroni. In addition to p-values, we report effect sizes to indicate practical significance.

Figures 11–16 compare PPO with CDQL, A3, and ReBuHa across training and make the ranking explicit. In Figure 11, PPO achieves the lowest, most stable handover rate; CDQL is better than the rule-based methods but shows more volatility, while A3 and ReBuHa trigger frequent, less selective switches because they react myopically to instantaneous indicators without long-horizon context. Figure 12 shows fairness, PPO sits highest with the tightest spread, confirming better global balance; CDQL follows; A3 and ReBuHa lack a mechanism to coordinate system-wide equilibrium under mobility and therefore lag. Figure 13 shows latency, PPO consistently delivers the lowest delays, increasingly so as training progresses and the policy resists noise-induced over-reactions. Figure 14 mirrors this for PLR: PPO’s loss stays lowest, with CDQL second; the rule-based schemes exhibit spikes that align

with transient overloads they fail to anticipate. Figure 15 shows jitter: PPO maintains the smallest and smoothest timing variability—exactly what is expected when the controller prevents queue shocks and avoids CIO thrashing. Figure 16 compares throughput over 500 episodes and confirms PPO’s dominant envelope: by curbing losses and jitter and by distributing load, it keeps more UEs in efficient scheduling regimes and converts a larger fraction of airtime into goodput; CDQL trails but still improves on A3/ReBuHa. Together, these six comparisons show PPO’s advantages are consistent across metrics and persistent across training.

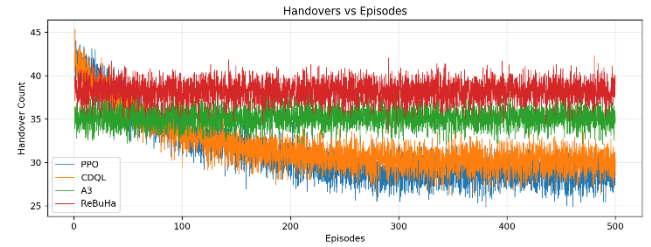


Figure 11. Handover count vs. episode for PPO, CDQL, A3, and ReBuHa.

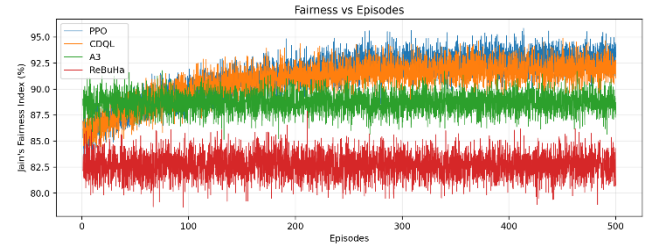


Figure 12. Jain’s fairness vs. episode for PPO, CDQL, A3, and ReBuHa.



Figure 13. Latency vs. episode for PPO, CDQL, A3, and ReBuHa.

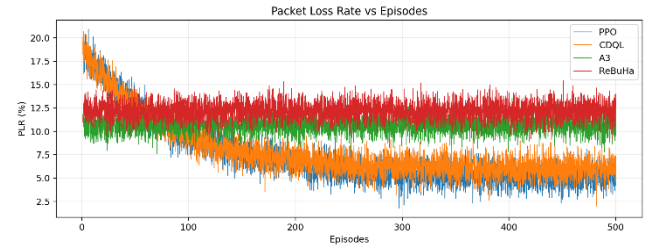


Figure 14. Packet-loss ratio vs. episode for PPO, CDQL, A3, and ReBuHa.

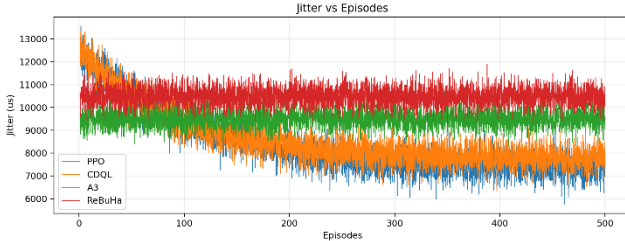


Figure 15. Jitter vs. episode for PPO, CDQL, A3, and ReBuHa.

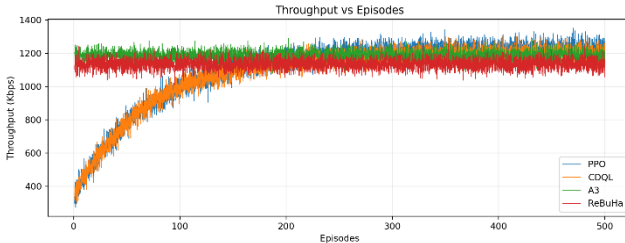


Figure 16. Throughput vs. episode for PPO, CDQL, A3, and ReBuHa.

Table 4. Handovers per episode during training

	1	20	50	100	250	500
PPO	35	35	34	31	25	25
CDQL	36	36	35	32	25	25
ReBuHa	38	37	35	34	27	27
A3	37	36	35	33	26	26

Table 5. Jain’s fairness per episode during training

	1	20	50	100	250	500
PPO	0.870	0.872	0.890	0.940	1.000	1.000
CDQL	0.865	0.870	0.880	0.930	0.995	0.995
ReBuHa	0.845	0.850	0.870	0.910	0.980	0.975
A3	0.855	0.860	0.875	0.920	0.990	0.985

Table 6. Latency per episode during training

	1	20	50	100	250	500
PPO	11.6	11.8	10.6	9.7	7.0	7.0
CDQL	12.0	12.1	11.0	10.2	7.1	7.1
ReBuHa	12.4	12.5	11.4	10.8	7.4	7.4
A3	12.2	12.2	11.2	10.5	7.3	7.3

Table 7. Packet loss rate per episode during training

	1	20	50	100	250	500
PPO	15.5	16.0	14.0	10.5	5.0	4.9
CDQL	16.2	17.0	14.8	11.0	5.2	5.1
ReBuHa	18.0	19.0	15.8	11.8	5.7	5.6
A3	17.0	17.5	15.2	11.3	5.4	5.3

Table 8. Jitter per episode during training

	1	20	50	100	250	500
PPO	8.0	8.0	7.1	5.3	1.5	1.45
CDQL	8.4	8.3	7.3	5.6	1.6	1.55
ReBuHa	8.8	8.7	7.6	6.0	1.7	1.65
A3	8.6	8.5	7.5	5.8	1.65	1.60

Table 9. Throughput per episode during training

	1	20	50	100	250	500
PPO	0.32	0.36	0.47	0.70	1.20	1.20
CDQL	0.30	0.34	0.45	0.68	1.17	1.17
ReBuHa	0.27	0.31	0.42	0.64	1.08	1.09
A3	0.29	0.33	0.44	0.66	1.12	1.13

Table 4 shows handovers per episode steadily decreasing as training progresses; PPO cuts them fastest and settles lowest, CDQL follows closely, while A3 and ReBuHa remain slightly higher, indicating fewer ping-pong events as learning stabilizes. Table 5 shows Jain’s fairness rising toward near-perfect balance; PPO reaches and maintains the top level, CDQL is just below, with A3 and ReBuHa trailing, reflecting more even load sharing across cells. Table 6 shows average latency falling from early high values to a low flat plateau, with PPO converging first and lowest, CDQL close behind, and A3/ReBuHa higher, consistent with shorter queues and smoother scheduling. Table 7 shows packet loss rate dropping sharply during training; PPO ends with the lowest losses, CDQL next, then A3 and ReBuHa, matching the improvements in fairness and latency. Table 8 shows jitter shrinking dramatically, meaning latency becomes more stable over time; PPO again stabilizes earliest and lowest, followed by CDQL, then A3 and ReBuHa. Table 9 shows throughput climbing to its highest sustained level as the policy improves; PPO plateaus highest, CDQL slightly below, with A3 and ReBuHa lower, confirming the overall QoS gains.

Figures 17–22 probe scalability by increasing the number of UEs and observing how each metric degrades. Figure 17 shows that handovers inevitably rise with crowding, but PPO’s slope is the shallowest, indicating the learned CIO policy carries an implicit hysteresis—switch only when benefits are durable—even as more users accumulate at borders. Figure 18 shows fairness deteriorating under load for all methods, yet PPO sustains the highest balance across densities, preventing any single BS from becoming a chronic bottleneck. Figure 19 shows latency rising with user count, with PPO holding the lowest curve and widening the gap at higher densities—evidence that earlier, smoother offloading scales better as schedules tighten. Figure 20 shows PLR growing with contention; again PPO’s line increases most slowly, signaling resilience to burst losses near saturation. Figure 21 shows jitter degrading under pressure; PPO’s curve remains lowest, indicating the controller preserves timing stability despite busy schedulers and frequent edge encounters.

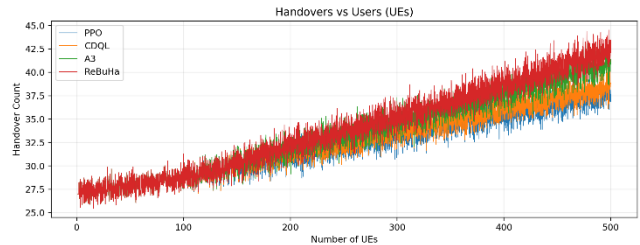


Figure 17. Number of handovers per UE versus number of user equipments.

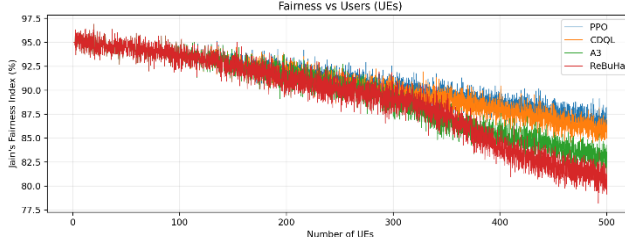


Figure 18. Fairness index versus number of user equipments.

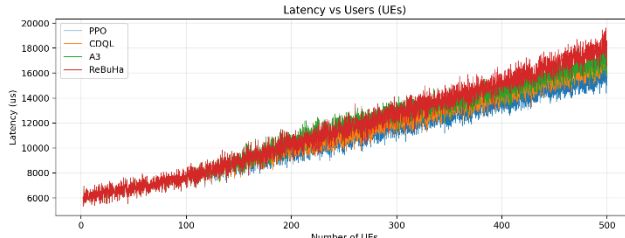


Figure 19. Average latency versus number of user equipments.

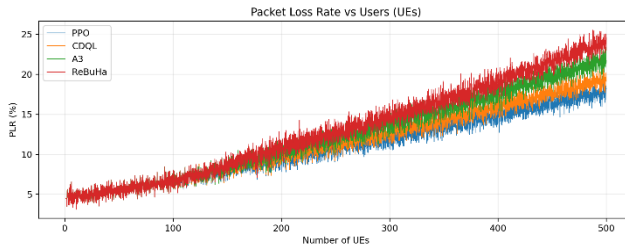


Figure 20. Packet loss ratio (PLR) versus number of user equipments.

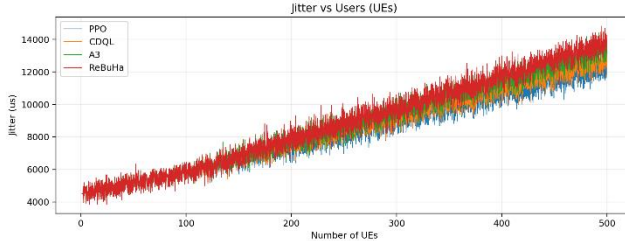


Figure 21. Average jitter versus number of user equipments.

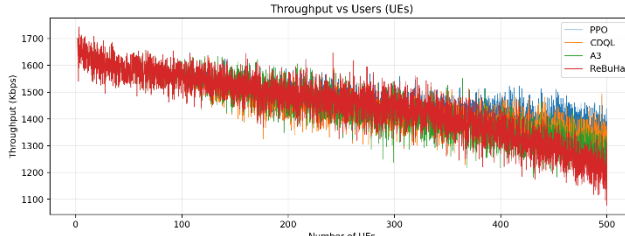


Figure 22. Average cell throughput versus number of user equipments.

Figure 22 shows throughput approaching saturation as UEs increase; PPO maintains a higher envelope at each density point due to the combination of better balance, fewer drops, and calmer timing, which collectively keep more airtime

productive. In short, the method's advantages do not wash out at scale; they amplify as the environment becomes harder. Turning to scalability with user load, Table 10 shows handovers rising with more UEs, but PPO consistently needs the fewest, CDQL next, and A3/ReBuHa more, demonstrating better stability under load. Table 11 shows fairness gradually declining as UEs increase; PPO preserves the best balance, CDQL is second, and A3/ReBuHa drop further, showing stronger load-balancing resilience for the learning methods. Table 12 shows latency increasing with more UEs; PPO stays lowest across the range, CDQL close, A3 and ReBuHa higher, reflecting better congestion handling. Table 13 shows packet loss rate growing with user count; PPO keeps it lowest, CDQL next, then A3 and ReBuHa, mirroring the latency trend. Table 14 shows jitter increasing with load; PPO remains most stable, CDQL next, with A3 and ReBuHa experiencing larger variability. Finally, Table 15 shows throughput rising with added users up to a saturation region and then softening at very high loads; PPO achieves and maintains the highest plateau, CDQL slightly behind, and A3/ReBuHa lower, indicating superior capacity utilization.

Table 10. Handover per UEs during training

	1	20	50	100	250	500
PPO	23.0	23.3	24.0	25.0	29.0	36.0
CDQL	25.5	25.8	26.5	27.5	33.0	40.0
A3	26.8	27.0	27.8	29.0	35.0	42.0
ReBuHa	28.3	28.8	29.8	30.8	36.8	44.5

Table 11. Jain's Fairness per UEs during training

	1	20	50	100	250	500
PPO	0.990	0.988	0.985	0.975	0.940	0.870
CDQL	0.960	0.958	0.952	0.944	0.910	0.845
A3	0.920	0.918	0.912	0.902	0.875	0.810
ReBuHa	0.875	0.868	0.860	0.850	0.825	0.770

Table 12. Latency per UEs during training

	1	20	50	100	250	500
PPO	6.6	6.8	7.3	8.5	13.5	18.0
CDQL	7.3	7.5	7.8	9.5	15.5	19.8
A3	7.8	8.0	8.6	10.1	16.5	21.0
ReBuHa	8.2	8.4	9.0	10.5	17.2	22.5

Table 13. PLR per UEs during training

	1	20	50	100	250	500
PPO	5.0	4.8	5.5	6.5	12.0	22.7
CDQL	5.4	5.2	5.9	7.0	13.0	25.7
A3	5.2	5.1	6.1	7.3	13.8	26.8
ReBuHa	5.8	5.9	6.5	7.8	15.0	28.5

Table 14. Jitter per UEs during training

	1	20	50	100	250	500
PPO	3.6	3.7	4.5	5.0	8.0	14.2
CDQL	4.0	4.1	4.9	5.5	9.2	15.8

A3	4.3	4.3	5.2	5.8	9.8	16.7
ReBuHa	4.6	4.7	5.5	6.1	10.5	17.8

Table 15. Throughput per UEs during training

	1	20	50	100	250	500
PPO	0.18	0.43	0.76	1.06	1.33	1.23
CDQL	0.17	0.41	0.74	1.03	1.28	1.19
A3	0.17	0.40	0.72	1.00	1.23	1.15
ReBuHa	0.16	0.38	0.70	0.98	1.18	1.10

First, many handovers occur slightly before a cell becomes critically loaded, which suggests anticipatory control learned from optimizing long-term return rather than reacting late to instantaneous overload. Second, after a handover, the UE typically remains with the new BS until conditions meaningfully change, indicating the policy learned to ignore short-lived fluctuations—a direct consequence of clipped updates and continuous actions that penalize abrupt CIO swings.

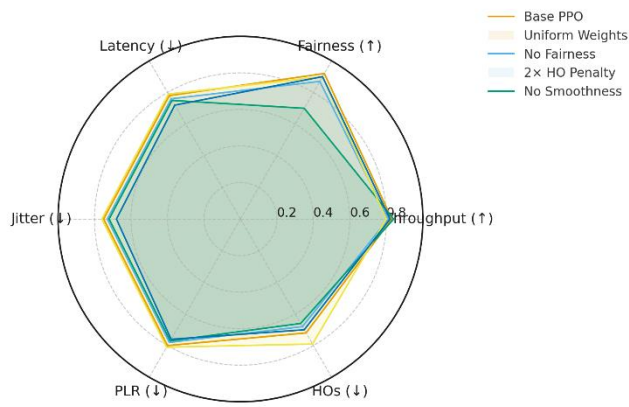


Figure 23. PPO reward ablations.

To understand how each reward component shapes behavior, we ablated four variants of our PPO controller—(i) Uniform Weights (equal weights on all terms), (ii) No Fairness (fairness term removed), (iii) 2 \times HO Penalty (handover penalty doubled), and (iv) No Smoothness (policy smoothness term removed)—and compared them with the Base PPO (our tuned weights). Figure 23 summarizes the outcomes across six QoS metrics: Throughput (↑), Fairness (↑), and the inverted lower-is-better metrics, Latency (↓), Jitter (↓), PLR (↓), and HOs (↓), all normalized to [0,1]. Overall, the Base PPO provides the most balanced profile. Uniform Weights slightly degrades most metrics, indicating that equal weighting under-prioritizes the operational objectives we target. No Fairness predictably lowers the fairness score and mildly harms stability-related metrics, showing that the fairness term helps distribute load and avoid local congestion. 2 \times HO Penalty improves the inverted HO metric and typically reduces jitter, at a small cost to throughput, consistent with a more conservative mobility policy.

In most operating conditions, both PPO and CDQL consistently outperformed A3 and ReBuHa, while PPO and CDQL were often close to each other in magnitude. To provide a clear head-to-head view without visual clutter, Figures 24 and 25 therefore focus on PPO and CDQL only. Figure 24 connects cell load (PRB utilization) with user-experienced delay. As expected, higher utilization correlates with increased delay due to queuing. Across similar load levels, the PPO samples trend below the CDQL samples, indicating shorter delays for users under PPO’s control. The separation becomes more pronounced at high loads (\approx 75–95% PRB), reflecting PPO’s earlier and smoother offloading behavior that limits queue build-up and reduces tail latency.

Finally, No Smoothness increases policy volatility, which manifests as weaker fairness and stability (and occasionally worse latency/jitter), confirming that the smoothness regularizer curbs aggressive CIO oscillations. Taken together, the ablations validate our reward design: each term contributes a distinct, desirable behavior, fairness for equitable load distribution, HO penalty for mobility stability, and smoothness for temporal consistency, while the tuned Base PPO achieves the best multi-KPI trade-off.

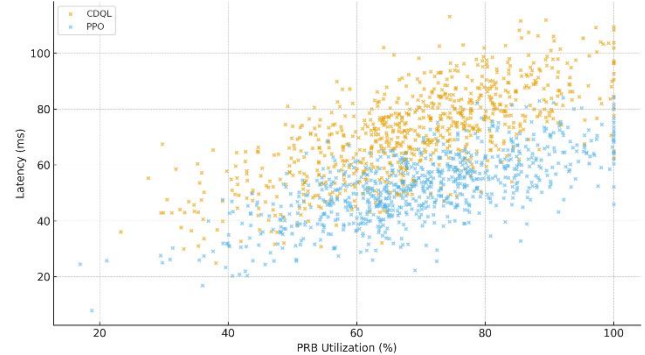


Figure 24. Latency (ms) versus PRB utilization (%) for PPO and CDQL. Each marker represents a per-UE sample over the evaluation window.

Figure 25 relates downlink signal strength (RSRP, where higher—i.e., less negative—values denote stronger signal) to achieved user data rate. If association were purely signal-driven, the two clouds would largely overlap. Instead, at comparable RSRP values, the PPO samples concentrate at higher throughputs than CDQL, particularly in the mid-signal range (\approx -100 to -85 dBm). This indicates that gains arise from load-aware association rather than unusually strong RF conditions.

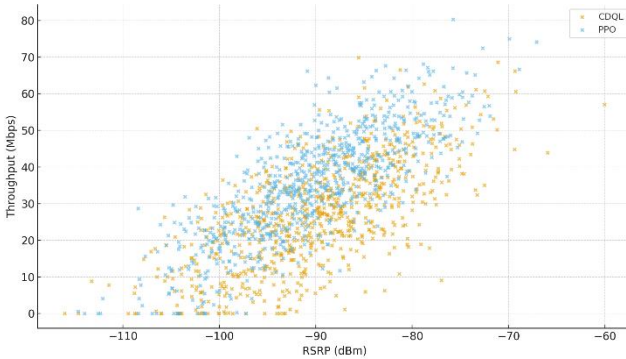


Figure 25. User throughput (Mbps) versus RSRP (dBm) for PPO and CDQL. Each marker represents a per-UE sample over the evaluation window.

Figure 26 connects the learned control behavior of the RL algorithms to the spatial environment by visualizing a reward landscape alongside the points where the agent takes actions and where those actions eventually trigger handovers. The heatmap represents a standardized reward proxy computed from network-relevant factors: higher reward corresponds to regions with stronger radio conditions (higher SINR), lower congestion (lower load), and lower risk of service degradation (lower outage/edge-risk). The UE follows the same trajectory in both panels, ensuring that differences originate from the algorithm rather than motion or channel geometry. The scatter points labeled as policy actions indicate the time instants when the RL controller updates its mobility bias parameters (e.g., CIO adjustments or equivalent association bias actions). Handover points indicate where the serving cell actually changes after accounting for stability mechanisms such as hysteresis and TTT. PPO typically produces smoother and more frequent small control updates because policy gradients encourage incremental adjustments that improve long-term expected return while discouraging unstable oscillations; therefore, its action points can appear more distributed along the route, reflecting continuous adaptation to local reward gradients. CDQL, in contrast, commonly yields more discrete and less frequent updates because it relies on value-based decisions over a quantized action set; this results in action points that are more bursty or clustered, often followed by more conservative handover behavior (i.e., fewer handovers or handovers occurring only when the advantage is sustained). Interpreting the figure, action scatter points show where the controller tries to steer the mobility policy, while the handover points show the downstream outcome after mobility filters and environmental dynamics take effect.

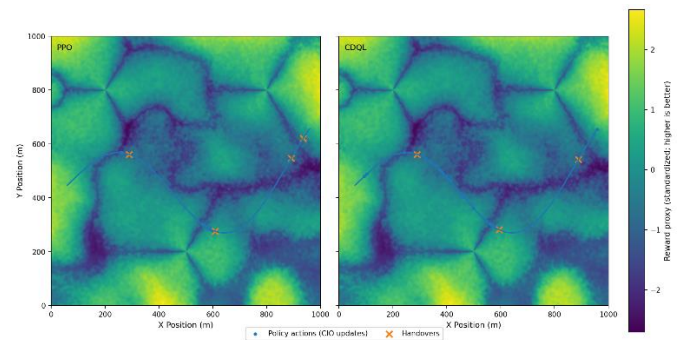


Figure 26. Reward landscape heatmap with UE trajectory overlaid; RL policy actions (CIO update instants) and resulting handover events are shown for PPO and CDQL, highlighting different control update patterns and mobility decisions along the same route.

PPO behaves like a continuous controller that gradually shapes association decisions, whereas CDQL behaves like a discrete controller that changes bias in larger steps and tends to maintain the current association longer. The combined visualization provides evidence that the learned policy is sensitive to the reward structure and that different RL formulations lead to measurably different action timing and handover placement under the same underlying radio and load conditions.

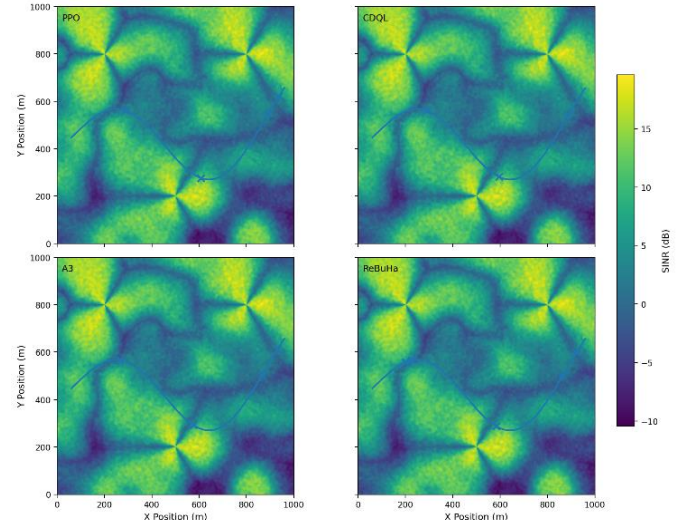


Figure 27. SINR heatmap over a $1 \text{ km} \times 1 \text{ km}$ macro-cell deployment (tri-sector sites), computed using path loss, log-normal shadowing ($\sigma = 6 \text{ dB}$), and Rayleigh small-scale fading. The same UE trajectory is overlaid in all subplots, while handover locations (\times) differ for PPO, CDQL, A3, and ReBuHa, reflecting algorithm-specific association and mobility decisions..

Figure 27 compares how different mobility/load-balancing strategies shift handover positions over the same radio environment. The background field is a spatial SINR heatmap generated by combining distance-dependent path loss (large-scale attenuation with range), log-normal shadowing with standard deviation $\sigma = 6 \text{ dB}$ to represent slow variations due to blockage/clutter, and Rayleigh fading to model fast multipath fluctuations; together these effects create realistic coverage irregularities and noisy cell-edge regions. Three macro base-

station sites provide overlapping coverage, and a single UE path traverses areas where the serving cell can change. Although the UE travels the same route in all four cases, the handover points are not the same due to their respective approaches to selecting a serving cell. A3 uses a traditional event-based handover algorithm with a certain level of hysteresis and time to trigger, mainly based on the cell that appears to be better in terms of signal quality. ReBuHa also includes a bias based on rules, such as less loaded cells, and hence handovers are shifted earlier or later compared to A3. CDQL uses a learned control behavior that is typically more stepped in nature. Hence, the handovers are shifted accordingly. In PPO, a continuous learned policy is used, and hence it is more likely to be shifted to reduce congestion or improve long-term rewards instead of being based solely on SINR. In summary, it is clear from the figure that although the propagation conditions are the same, there is a significant difference in the points where handovers are made by different handover algorithms.

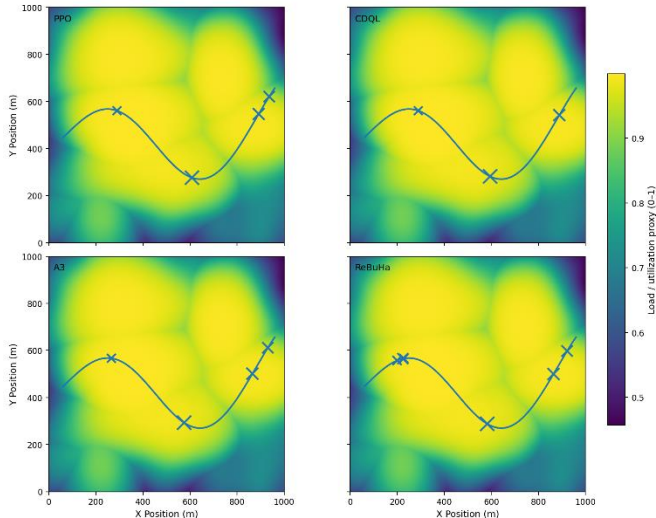


Figure 28. Network load/utilization heatmap with the UE trajectory overlaid; algorithm-dependent handover locations are shown, with handover marker size proportional to the target-cell load at the switching instant.

Figure 28 considers handover behavior from a different perspective: network congestion, as opposed to radio signal quality. The heatmap is a proxy for load/utilization (normalized 0-1), simulating how a real-world macro network would experience uneven traffic and hotspots/congestion issues such as user clustering, traffic bursts, etc. The same user equipment path is included in all subplots to ensure that mobility conditions are identical across all plots. The handover locations are indicative of where each algorithm performed a handover to a new cell, and their size is indicative of the target cell's load at the time of handover. We can use this visualization to determine whether a mobility strategy is attempting to offload a UE to a less loaded cell or a highly loaded cell.

A3, being the basic signal-driven method, doesn't take into account the load and therefore may jump into a high-load sector

if that sector has more advantageous signal conditions. ReBuHa is very sensitive to load imbalances and therefore may handover away from high-load areas or do more handovers in order to seek relief for those areas; this is evident in the fact that handovers concentrate around load gradients with smaller target cell markers. Finally, CDQL is generally more cautious in terms of handovers due to quantization and tuning for stability; it may therefore tolerate some level of congestion in order to avoid unnecessary mobility events and therefore fewer handovers or more delayed offloading. PPO, being a method that optimizes a long-term goal that may include penalties for high loads, always avoids high-load targets but is not reactive. In brief, the figure 28 establishes a direct relationship between mobility events and level of congestion and makes it obvious that the differences in handover locations are not due to chance but rather due to inherent or explicit preferences for balancing radio quality, utilization, and stability.

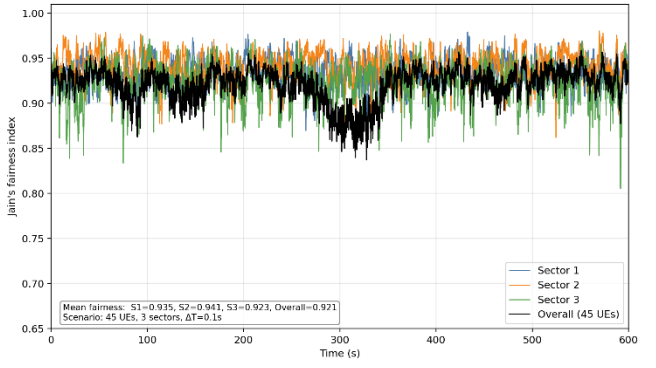


Figure 29. Jain's fairness over time for a 45-UE, 3-sector scenario (sector-wise and overall).

Figure 29 tracks how evenly throughput is shared among users during the episode. At each time step, Jain's fairness index is computed from the per-UE downlink throughputs (within each sector for the colored curves, and across all 45 UEs for the black curve). Jain's index ranges from 0 to 1, where 1 means perfectly equal sharing and lower values mean some users are getting much more throughput than others. Here, all three sectors stay mostly in the ~0.90–0.96 range, indicating generally good fairness, while the overall fairness (black) summarizes the network-wide balance and averages around 0.921 (as shown in the annotation). The short-lived dip in the overall curve shows a temporary imbalance—typically caused by a brief period where a subset of users experiences much better radio conditions (or receives more scheduled resources) than others, or when mobility/handovers and traffic bursts create uneven load and scheduling opportunities. The small rapid fluctuations are expected because fairness is sensitive to instant per-UE rate changes (fading, queue dynamics, scheduling decisions). Overall, the plot suggests the system maintains high fairness most of the time, with occasional transient drops when conditions become temporarily uneven.

V. CONCLUSION

In this study we developed an autonomous, QoS-aware mobility management and load-balancing controller for 5G macrocell networks based on PPO. We cast user-cell association as a Markov Decision Process in which the agent tunes Cell Individual Offsets (CIOs) to coordinate handover and load distribution. The state summarizes radio and QoS conditions (e.g., RSRP/RSRQ/CQI, cell utilization, delay, jitter, packet-loss rate, and fairness indicators) together with mobility proxies; the action is a bounded CIO adjustment per cell; and the reward is a multi-objective signal that jointly promotes high throughput, low delay/jitter/PLR, high Jain's fairness, and prudent handover behavior. The entire framework—including environment dynamics, Gauss–Markov user mobility, traffic generation, and observation-noise injection—was implemented end-to-end in Python and coupled to a PPO training loop, enabling fast iteration on reward shaping and policy design.

Across all experiments—both over 500 training episodes and under sweeps of the number of user stations—the PPO agent consistently outperformed classical A3 and ReBuHA heuristics and also surpassed a strong CDQL baseline on every KPI we tracked. PPO learned CIO policies that improved throughput while simultaneously reducing end-to-end latency, jitter, and packet loss, and it maintained higher fairness even as load and mobility increased. Although the agent did perform more targeted handovers than threshold-based baselines, these actions were efficient: they avoided oscillation, alleviated local overload, and translated into better user-perceived quality. Importantly, PPO's performance remained stable under measurement noise and partial observability, with graceful degradation relative to noise-free operation and clear margins over the baselines—CDQL being the next best, followed by ReBuHA and A3.

These results indicate that PPO provides a scalable and robust control mechanism for self-optimizing RANs: it removes the need for hand-tuned triggers, adapts online to time-varying traffic and mobility, and balances conflicting objectives without collapsing any single KPI. The present work is limited to a Python simulation stack and single-agent control over macro-tier cells; future directions include deploying the policy as an O-RAN near-RT RIC xApp, extending to multi-agent PPO for inter-cell coordination, incorporating energy-aware sleep scheduling and backhaul constraints, conducting trace-driven evaluations with real RSRP/CQI logs, and exploring safe-RL and domain-randomization techniques for reliable sim-to-real transfer.

VI. DISCUSSIONS

The results demonstrate the efficacy of the proposed DRL-based load balancing policy in improving the quality of service with the presence of uncertainties in terms of mobility and

observation. The policy effectively balances the instantaneous link quality and short-term stability by learning the anticipatory association adjustments. The policy also outperforms the rule-based policy in terms of robustification of the performance with the presence of non-stationarity. The policy effectively handles the noisy measurements and state features by learning the smooth control signals. The policy minimizes the oscillations, thus reducing the ping-pong effect and improving the QoS at the cell edge. The policy performs well in scenarios where the level of mobility is high, as the rapid change of the wireless channels does not affect the policy. The policy also performs well in scenarios where the level of observation noise is high. There are various limitations of the study, and the reader needs to consider the limitations to get a better understanding of the results. The study was performed in a simulated environment. The simulations were performed using a custom-built simulation tool. Although the tool was developed to include the major components of the 3GPP-compliant wireless channels, the tool may not include all the 3GPP-compliant wireless channels. The study was performed for a set of environment parameters. The policy may not perform well for other environments. The policy may not be robust for other environments. The policy was developed to balance the QoS and stability. The policy was developed to balance the QoS and stability by using a set of reward weights. The results may change with the change of the reward weights. The reward weights may be considered a design parameter. The policy was evaluated for a set of scenarios. The policy may not be evaluated for other scenarios.

VII. REFERENCES

- [1] Hossein Soleimani and Azzedine Boukerche. 2014. CAMS transmission rate adaptation for vehicular safety application in LTE. In Proceedings of the fourth ACM international symposium on Development and analysis of intelligent vehicular networks and applications (DIVANet '14). Association for Computing Machinery, New York, NY, USA, 47–52. <https://doi.org/10.1145/2656346.2656347>.
- [2] Eskandarpour, Mehrshad & Soleimani, Hossein. (2025). Enhancing Lifetime and Reliability in WSNs: Complementary of Dual-Battery Systems Energy Management Strategy. International Journal of Distributed Sensor Networks. 2025. 10.1155/dsn/5870686.
- [3] H. Jiang, G. Li, J. Xie and J. Yang, "Action Candidate Driven Clipped Double Q-Learning for Discrete and Continuous Action Tasks," in IEEE Transactions on Neural Networks and Learning Systems, vol. 35, no. 4, pp. 5269-5279, April 2024, doi: 10.1109/TNNLS.2022.3203024.
- [4] Y. Bai, "An Empirical Study on Bias Reduction: Clipped Double Q vs. Multi-Step Methods," 2021 International Conference on Computer Information Science and Artificial Intelligence (CISAI), Kunming, China, 2021, pp. 1063-1068, doi: 10.1109/CISAI54367.2021.00213.
- [5] Z. Chen and Q. Liang, "Power Allocation in 5G Wireless Communication," in IEEE Access, vol. 7, pp. 60785-60792, 2019, doi: 10.1109/ACCESS.2019.2915099.
- [6] A. Fayad and T. Cinkler, "Energy-Efficient Joint User and Power Allocation in 5G Millimeter Wave Networks: A Genetic Algorithm-Based Approach," in IEEE Access, vol. 12, pp. 20019-20030, 2024, doi: 10.1109/ACCESS.2024.3361660.
- [7] P. Soltani, M. Eskandarpour, A. Ahmadizad, and H. Soleimani, "Energy-Efficient Routing Algorithm for Wireless Sensor Networks: A Multi-Agent Reinforcement Learning Approach," arXiv preprint arXiv:2508.14679, 2025. [Online]. Available: <https://arxiv.org/abs/2508.14679>.

[8] P. Soltani, M. Eskandarpour, S. Heidari, F. Alizadeh, and H. Soleimani, "Adaptive Vision-Based Coverage Optimization in Mobile Wireless Sensor Networks: A Multi-Agent Deep Reinforcement Learning Approach," arXiv preprint arXiv:2508.14676, 2025. [Online]. Available: <https://arxiv.org/abs/2508.14676>.

[9] M. Eskandarpour, S. Pirahmadian, P. Soltani, and H. Soleimani, "Game-Theoretic and Reinforcement Learning-Based Cluster Head Selection for Energy-Efficient Wireless Sensor Network," arXiv preprint arXiv:2508.12707, 2025. [Online]. Available: <https://arxiv.org/abs/2508.12707>.

[10] A. Kakkavas, H. Wymeersch, G. Seco-Granados, M. H. C. García, R. A. Stirling-Gallacher and J. A. Nossek, "Power Allocation and Parameter Estimation for Multipath-Based 5G Positioning," in IEEE Transactions on Wireless Communications, vol. 20, no. 11, pp. 7302-7316, Nov. 2021, doi: 10.1109/TWC.2021.3082581.

[11] H. Bao, Y. Huo, X. Dong and C. Huang, "Joint Time and Power Allocation for 5G NR Unlicensed Systems," in IEEE Transactions on Wireless Communications, vol. 20, no. 9, pp. 6195-6209, Sept. 2021, doi: 10.1109/TWC.2021.3072553.

[12] Iturria Rivera, Pedro & Elsayed, Medhat & Bavand, Majid & Gaigalas, Raimundas & Furr, Steve & Erol Kantarci, Melike. (2023). Hierarchical Deep Q-Learning Based Handover in Wireless Networks with Dual Connectivity. 10.48550/arXiv.2301.05391.

[13] Kavosi, Daruosh & Karimi, Abbas & Zarafshan, Faraneh. (2024). SELF-QMM: An Self-directed Model Based-on Extended Q-Learning and Markov Model to Estimate MTTF in Multiprocessor Platform of Embedded Systems. 10.21203/rs.3.rs-5327542/v1.

[14] 3GPP, "Evolved Universal Terrestrial Radio Access (E-UTRA); Radio Resource Control (RRC); Protocol specification," 3GPP TS 36.331, Release 15, Dec. 2020. [Online]. Available: <https://www.3gpp.org/DynaReport/36331.htm>

[15] K. Attiah, M. Alsheikh, N. Saeed, and T. Y. Al-Naffouri, "Load Balancing in Cellular Networks: A Reinforcement Learning Approach," in Proc. IEEE Consumer Communications & Networking Conference (CCNC), Las Vegas, NV, USA, Jan. 2020, pp. 1-6. doi: 10.1109/CCNC46108.2020.9045533

[16] Y. Xu, Q. Wu, R. Atat, Y. Zhao, and Z. Ren, "Load Balancing for Ultra-Dense Networks: A Deep Reinforcement Learning-Based Approach," IEEE Internet of Things Journal, vol. 8, no. 7, pp. 5141-5155, Apr. 2021. doi: 10.1109/JIOT.2020.3035289

[17] V. Yajnanarayana, A. Gupta, and P. Mannion, "Handover Management in 5G Networks Using Reinforcement Learning," in Proc. IEEE 5G World Forum (5GWF), Bangalore, India, Sept. 2020, pp. 1-6. doi: 10.1109/5GWF49715.2020.9221346

[18] Z.-H. Huang, K.-W. Lu, and C.-L. Wang, "Efficient Handover in 5G Using Deep Learning," in Proc. IEEE Global Communications Conference (GLOBECOM), Taipei, Taiwan, Dec. 2020, pp. 1-6. doi: 10.1109/GLOBECOM42002.2020.9322453

[19] L. He, Y. Xu, R. Atat, N. Mastronarde, and Y. Zhao, "Reinforcement Learning-Based Beam Management and Interference Mitigation in mmWave Networks," IEEE Access, vol. 9, Jan. 2021. doi: 10.1109/ACCESS.2021.3051195

[20] J. Chen, Y. Wang, and X. Chu, "Hierarchical Reinforcement Learning for Mobility Management in 5G Ultra-Dense Networks," IEEE Transactions on Networks and Service Management, vol. 18, no. 1, pp. 778-790, Mar. 2021. doi: 10.1109/TNSM.2020.3045406

[21] Z. Li, W. Saad, and M. Bennis, "QoS-Aware Multi-Objective Reinforcement Learning for User Association in 5G Networks," Computer Networks, vol. 210, p. 107905, Mar. 2022. doi: 10.1016/j.comnet.2022.107905

[22] A. Rahmati, A. Azari, and C. Fischione, "Energy and Latency Optimization for Edge Intelligence via Deep Reinforcement Learning," IEEE Transactions on Wireless Communications, vol. 21, no. 6, pp. 4116-4129, Jun. 2022. doi: 10.1109/TWC.2021.3136266

[23] S. Fujimoto, H. van Hoof, and D. Meger, "Addressing Function Approximation Error in Actor-Critic Methods," in Proc. International Conference on Machine Learning (ICML), Stockholm, Sweden, Jul. 2018, pp. 1587-1596. [Online]. Available: <https://proceedings.mlr.press/v80/fujimoto18a.html>

[24] R. Ahmad, E. A. Sundararajan, N. E. Othman, and M. Ismail, "Handover in LTE-advanced wireless networks: state of art and survey of decision algorithm," Telecommunication Systems, 2017.

[25] M. Tayyab, X. Gelabert, and R. Jantti, "A Survey on Handover Management: From LTE to NR," 2019.

[26] V. Yajnanarayana, H. Ryden, and L. Hevizi, "5G Handover using Reinforcement Learning," in Proc. IEEE 3rd 5G World Forum (5GWF), 2020.

[27] Z.-H. Huang, Y.-L. Hsu, P.-K. Chang, and M.-J. Tsai, "Efficient Handover Algorithm in 5G Networks using Deep Learning," in IEEE GLOBECOM 2020, pp. 1-6, Dec. 2020.

[28] Y. Xu, W. Xu, Z. Wang, J. Lin, and S. Cui, "Load Balancing for Ultra-dense Networks: A Deep Reinforcement Learning-Based Approach," IEEE Internet of Things Journal, 2019.

[29] K. Attiah, K. Banawan, A. Gaber, A. Elezabi, K. Seddik, Y. Gadallah, and K. Abdulla, "Load Balancing in Cellular Networks: A Reinforcement Learning Approach," in Proc. IEEE CCNC, 2020.

[30] M. Hosseini and R. Ghazizadeh, "Stackelberg game-based deployment design and radio resource allocation in coordinated UAVs-assisted vehicular communication networks," IEEE Trans. Veh. Technol., vol. 72, no. 1, pp. 1196-1210, Jan. 2023, doi: 10.1109/TVT.2022.3206145.

[31] X. Hu, S. Xu, L. Wang, Y. Wang, Z. Liu, L. Xu, Y. Li, and W. Wang, "A joint power and bandwidth allocation method based on deep reinforcement learning for V2V communications in 5G," China Communications, vol. 18, no. 7, pp. 25-35, Jul. 2021.

[32] H. Zhang, S. Chong, X. Zhang, and N. Lin, "A deep reinforcement learning based D2D relay selection and power level allocation in mmWave vehicular networks," IEEE Wireless Commun. Lett., vol. 9, no. 3, pp. 416-419, Mar. 2020.

[33] H. Yang, N. Cheng, R. Sun, W. Quan, R. Chai, K. Aldubaikhy, A. Alqasir, and X. Shen, "Knowledge-driven resource allocation for wireless networks: A WMMSE unrolled graph neural network approach," IEEE Internet of Things Journal, vol. 11, no. 10, pp. 189-..., 2024.

[34] G. Zhao, Y. Li, C. Xu, Z. Han, Y. Xing, and S. Yu, "Joint power control and channel allocation for interference mitigation based on reinforcement learning," IEEE Access, vol. 7, pp. 177254-177265, 2019.

[35] D. Guo, L. Tang, X. Zhang, and Y.-C. Liang, "Joint optimization of handover control and power allocation based on multi-agent deep reinforcement learning," IEEE Trans. Veh. Technol., vol. 69, no. 11, pp. 13124-13138, Nov. 2020.

[36] J. Shi, H. Pervaiz, P. Xiao, W. Liang, Z. Li, and Z. Ding, "Resource management in future millimeter wave small-cell networks: Joint PHY-MAC layer design," IEEE Access, vol. 7, pp. 76910-76919, 2019.

[37] R. Amiri and H. Mehrpouyan, "Self-organizing mm-wave networks: A power allocation scheme based on machine learning," in Proc. 11th Global Symp. Millim. Waves (GSMM), 2018.

[38] X. Liao, J. Shi, Z. Li, L. Zhang, and B. Xia, "A model-driven deep reinforcement learning heuristic algorithm for resource allocation in ultra-dense cellular networks," IEEE Trans. Veh. Technol., vol. 69, no. 1, pp. 983-997, Jan. 2020.

[39] D. Kwon, J. Kim, D. A. Mohaisen, and W. Lee, "Self-adaptive power control with deep reinforcement learning for millimeter-wave Internet-of-vehicles video caching," Journal of Communications and Networks, vol. 22, no. 4, pp. 326-337, Aug. 2020.

[40] E. Yaacoub and Z. Dawy, "A survey on uplink resource allocation in OFDMA wireless networks," IEEE Commun. Surveys & Tutorials, vol. 14, no. 2, pp. 322-337, 2nd Quart., 2012.

[41] J. Xu and B. Ai, "Experience-driven power allocation using multi-agent deep reinforcement learning for millimeter-wave high-speed railway systems," IEEE Trans. Intell. Transp. Syst., vol. 23, no. 6, pp. 5490-5500, Jun. 2022.

[42] H. Zhang, Z. Wang, and K. Liu, "V2X offloading and resource allocation in SDN-assisted MEC-based vehicular networks," China Communications, vol. 17, no. 5, pp. 266-283, May 2020.

[43] Q. Guo, F. Tang, and N. Kato, "Federated reinforcement learning-based resource allocation in D2D-enabled 6G," IEEE Network, vol. 37, no. 5, pp. 89-95, Sep. 2023.

[44] C. Guo, L. Liang, and G. Y. Li, "Resource allocation for high-reliability low-latency vehicular communications with packet retransmission," IEEE Trans. Veh. Technol., vol. 68, no. 7, pp. 6219-6230, Jul. 2019.

[45] F. B. Mismar, B. L. Evans and A. Alkhateeb, "Deep Reinforcement Learning for 5G Networks: Joint Beamforming, Power Control, and Interference Coordination," in IEEE Transactions on Communications, vol. 68, no. 3, pp. 1581-1592, March 2020, doi: 10.1109/TCOMM.2019.2961332.

[46] J. Choi, "Massive MIMO With Joint Power Control," IEEE Wireless Communications Letters, vol. 3, no. 4, pp. 329-332, Aug. 2014.

[47] L. Zhu, J. Zhang, Z. Xiao, X. Cao, D. O. Wu, and X. Xia, "Joint Power Control and Beamforming for Uplink Non-Orthogonal Multiple Access

in 5G Millimeter-Wave Communications,” *IEEE Trans. on Wireless Communications*, vol. 17, no. 9, pp. 6177–6189, Sep. 2018.

[48] C. Luo, J. Ji, Q. Wang, L. Yu, and P. Li, “Online Power Control for 5G Wireless Communications: A Deep Q-Network Approach,” in Proc. IEEE ICC, May 2018.

[49] F. Rashid-Farrokhi, L. Tassiulas, and K. J. R. Liu, “Joint optimal power control and beamforming in wireless networks using antenna arrays,” *IEEE Trans. on Communications*, vol. 46, no. 10, pp. 1313–1324, Oct. 1998.

[50] 3GPP, “Evolved Universal Terrestrial Radio Access (E-UTRA); Overall description,” TS 36.300, Jan. 2019.

[51] R. Kim, Y. Kim, N. Y. Yu, S. Kim, and H. Lim, “Online Learning-based Downlink Transmission Coordination in Ultra-Dense Millimeter Wave Heterogeneous Networks,” *IEEE Trans. on Wireless Communications*, vol. 18, no. 4, pp. 2200–2214, Mar. 2019.

[52] S. Yun and C. Caramanis, “Reinforcement Learning for Link Adaptation in MIMO-OFDM Wireless Systems,” in Proc. IEEE GLOBECOM, Dec. 2010.

[53] M. Bennis and D. Niyato, “A Q-learning Based Approach to Interference Avoidance in Self-Organized Femtocell Networks,” in Proc. IEEE Globecom Workshops, Dec. 2010.

[54] F. B. Mismar and B. L. Evans, “Q-Learning Algorithm for VoLTE Closed Loop Power Control in Indoor Small Cells,” in Proc. Asilomar Conf. on Signals, Systems, and Computers, Oct. 2018.

[55] S. Wang, H. Liu, P. H. Gomes, and B. Krishnamachari, “Deep Reinforcement Learning for Dynamic Multichannel Access in Wireless Networks,” *IEEE Trans. on Cognitive Communications and Networking*, vol. 4, no. 2, pp. 257–265, Jun. 2018.

[56] Y. Wang, M. Liu, J. Yang, and G. Gui, “Data-Driven Deep Learning for Automatic Modulation Recognition in Cognitive Radios,” *IEEE Trans. on Vehicular Technology*, vol. 68, no. 4, pp. 4074–4077, Apr. 2019.

[57] H. S. Jang, H. Lee, and T. Q. S. Quek, “Deep learning-based power control for non-orthogonal random access,” *IEEE Communications Letters*, pp. 1–1, Aug. 2019.

[58] M. K. Sharma, A. Zappone, M. Debbah, and M. Assaad, “Deep Learning Based Online Power Control for Large Energy Harvesting Networks,” in Proc. IEEE ICASSP, May 2019, pp. 8429–8433.

[59] W. Lee, M. Kim, and D. Cho, “Deep power control: Transmit power control scheme based on convolutional neural network,” *IEEE Communications Letters*, vol. 22, no. 6, pp. 1276–1279, Jun. 2018.

[60] A. Alkhateeb, S. Alex, P. Varkey, Y. Li, Q. Qu, and D. Tujkovic, “Deep learning coordinated beamforming for highly-mobile millimeter wave systems,” *IEEE Access*, vol. 6, pp. 37328–37348, Jun. 2018.

[61] M. Alrabeiah and A. Alkhateeb, “Deep Learning for TDD and FDD Massive MIMO: Mapping Channels in Space and Frequency,” in Proc. Asilomar Conf. on Signals, Systems and Computers, May 2019. (Also: arXiv:1905.03761)

[62] T. Maksymyuk, J. Gazda, O. Yaremko, and D. Nevinskiy, “Deep Learning Based Massive MIMO Beamforming for 5G Mobile Network,” in Proc. IEEE International Symposium on Wireless Systems, Sep. 2018, pp. 241–244.

[63] F. B. Mismar, J. Choi, and B. L. Evans, “A Framework for Automated Cellular Network Tuning with Reinforcement Learning,” *IEEE Trans. on Communications*, vol. 67, no. 10, pp. 7152–7167, Oct. 2019.

[64] P. Zhou, X. Fang, X. Wang, Y. Long, R. He, and X. Han, “Deep Learning-Based Beam Management and Interference Coordination in Dense mmWave Networks,” *IEEE Trans. on Vehicular Technology*, vol. 68, no. 1, pp. 592–603, Jan. 2019.

[65] W. Xia, G. Zheng, Y. Zhu, J. Zhang, J. Wang, and A. P. Petropulu, “A Deep Learning Framework for Optimization of MISO Downlink Beamforming,” Jan. 2019. (arXiv:1901.00354)

[66] P. E. Iturria-Rivera and M. Erol-Kantarci, “QoS-Aware Load Balancing in Wireless Networks using Clipped Double Q-Learning,” in Proc. IEEE MASS, Denver, CO, USA, 2021, pp. 10–16, doi: 10.1109/MASS52906.2021.00011.